ADVANCED OPTICAL MATERIALS
www.advopticalmat.de

Template-Directed Solidification of Eutectic Optical Materials

*Ashish A. Kulkarni, Julia Kohanek, Kaitlin I. Tyler, Erik Hanson, Dong-Uk Kim, Katsuyo Thornton, and Paul V. Braun**

Mesostructured materials can exhibit enhanced light–matter interactions, which can become particularly strong when the characteristic dimensions of the structure are similar to or smaller than the wavelength of light. For controlling visible to near-infrared wavelengths, the small characteristic dimensions of the required structures usually demand fabrication by sophisticated lithographic techniques. However, these fabrication methods are restricted to producing 2D and a limited range of 3D structures. When a large volume of structured material is required, the primary approach is to use self-assembly, and the literature includes many examples of mesostructured optical materials formed via self-assembly. However, self-organized materials almost always contain structural imperfections which limit their performance. Emerging work, however, is showing that by performing self-assembly within a guiding template, the defect density in self-assembled structures can be reduced. Particularly interesting is the possibility that utilizing a template can result in the formation of mesostructures not present in either the template or the native self-organizing material. In this review, particular emphasis is placed on emerging results showing the effect of mesoscale templates on the microstructure of solidifying eutectic materials, with a specific focus on how template-directed solidification may be a powerful approach for fabricating optically active structures, including optical metamaterials.

1. Introduction

Photonic crystals (materials with periodic variations in optical properties in one, two, or three dimensions on the order of the wavelength of light) are widely utilized to manipulate light.[1] Example devices based on photonic crystals include distributed Bragg reflectors, diffraction gratings, wire-grid polarizers, some waveguides, and many lasers.[1–3] Materials with powerful optical functionalities, including negative-index of refraction and optical chirality, can be realized by appropriate placement of materials with suitable properties in 2D or 3D space.[4–6] Light in the visible spectrum can be manipulated, although the tolerance for defects is exceedingly low at visible frequencies, and the number of materials with the appropriate properties is limited.[7,8] Most photonic crystals are fabricated by high-resolution top-down 2D patterning methods such as electron-beam lithography, interference lithography, and focused ion beam milling.[9] However, it is challenging to fabricate large-area bulk materials with these techniques, especially with intricate internal structures.[8] Additionally, many materials with promising optical properties are not compatible with these top-down patterning methods.[4,10]

As work on colloidal crystals has shown, controlled self-assembly is an effective route to organizing materials into 3D architectures, which interact strongly with light.[9–13] Colloidal self-assembly, however, only offers a limited set of symmetries (generally those of close packed arrangements), and a spherical basis.[12] For many applications, considerably more complex structures are of interest. Particularly promising approaches for forming materials with complex internal microstructures include eutectic solidification and block copolymer self-assembly,[14–17] and materials with interesting optical properties have been reported using both approaches. These methods are advantageous due to the wide range of microstructures they form. Here, we focus on the structures formed by eutectic solidification since materials with a broader range of optical properties are available compared to that provided by block copolymers, and because the characteristic lengths of structures accessible through eutectic solidification better match the wavelengths of visible and IR light. Further, forming materials with sufficiently large characteristic dimensions for interaction with visible light by block copolymer assembly is synthetically challenging as it requires high molecular weight polymers.[18] Similarly, self-assembly of other building blocks, e.g., nanoparticles,[19,20] molecules,[21,22] and DNA,[23,24] tend to produce structures with characteristic dimensions too small to provide strong light–matter interactions (via diffractive phenomena),[2,3,25] and are thus not the emphasis of this review.

A. A. Kulkarni, J. Kohanek, K. I. Tyler, Prof. P. V. Braun
Department of Materials Science and Engineering
Frederick Seitz Materials Research Laboratory
Beckman Institute for Advanced Science and Technology
University of Illinois at Urbana-Champaign
Urbana, IL 61801, USA
E-mail: pbraun@illinois.edu
E. Hanson, Dr. D.-U. Kim, Prof. K. Thornton
Department of Materials Science and Engineering
University of Michigan
Ann Arbor, MI 48109, USA
The ORCID identification number(s) for the author(s) of this article can be found under https://doi.org/10.1002/adom.201800071.

DOI: 10.1002/adom.201800071

Here, we first introduce the idea of template design and replication, followed by a brief survey of where template-directed assembly has led to the emergence of optically promising microstructures. The core of this review focuses on eutectic systems for the central reason that even though there is a vast library of eutectic systems that have promising material combinations, and the solidification of eutectic materials has been well studied, their utilization for optical functionalities has not received sufficient attention to realize their full potential. Along with a discussion on optically interesting self-organized eutectic materials, we include examples of how phase-field modeling has been used to understand and guide the development of templates, leading to the formation of eutectic microstructures with enhanced optical properties. Finally, we discuss the underlying challenges and future opportunities for using template-directed eutectic solidification of optical materials, and provide our perspectives on the potential of template-directed solidification of eutectic materials for forming optical materials including optical metamaterials.

2. Templating Overview

Common in the natural world are materials with unique microstructures that exhibit properties considerably superior to homogeneous materials.[26–30] Many groups have investigated templating strategies (by utilizing a template to guide the structure of a material) to form synthetic materials with complex deterministic microstructures similar to those observed in the natural world.[31,32] The templating approach is attractive because most materials do not form complex deterministic structures naturally.[31] Techniques including electrodeposition, capillary action, sol–gel templating, and drop casting have all been used to infill preformed templates, enabling replication and/or inversion of the template geometry with the functional material of interest.[33–39] The goal is to synthesize new materials with properties that emerge from synergistic interactions of the inherent properties of the constituent materials and the template structure.[31,32,40,41] Along with photonic applications, template-replicated and inverted structures have also been used for electrochemical energy storage, sensing, and high-strength applications as discussed below.

Artificial opals, formed by self-assembly of silica or polymer colloidal particles, are perhaps the most common templates reported in the literature.[12,13,42] The size tunability and chemical stability of colloidal particles and the 3D structure of an artificial opal make it suitable for photonic applications.[42] Opal templates have been filled via numerous methods, with electrochemical deposition perhaps being the most versatile.[33,34,43] Metals, semiconductors, and oxides have all been grown in single-crystal and polycrystalline form within opal templates.[33,34,43] **Figure 1**A includes examples of opal templated Ni, CdSe, CdS, ZnO, and Cu_2O inverse opals.[33–35,43] The CdSe, CdS, ZnO, and Cu_2O-based systems are examples of how templating can be used to form high refractive-index photonic crystals. Ni inverse opals have also been used in a wide range of applications from scaffolds for graphene chemical vapor deposition, to support for electrochemically active materials in Li-ion battery electrodes.[43–45] As an example of templating of

Ashish A. Kulkarni is currently a doctoral candidate under the supervision of Prof. Paul V. Braun in the Department of Materials Science and Engineering at the University of Illinois Urbana-Champaign, USA. He received his B.Tech. degree in Metallurgical and Materials Engineering from Visvesvaraya National Institute of Technology Nagpur, India and M.Tech. degree in Materials Science from Indian Institute of Technology Kanpur, India. His current interest mainly focuses on the template-directed solidification of salt eutectics for optical applications.

Katsuyo Thornton is a Professor of Materials Science and Engineering at the University of Michigan, Ann Arbor. She holds a Ph.D. from the Department of Astronomy and Astrophysics at the University of Chicago. Prior to joining the faculty of the University of Michigan, she held postdoctoral and research assistant professor positions at Northwestern University and visiting lecturer and scientist positions at MIT. Thornton's research focuses on computational modeling of materials based on their thermodynamics and kinetics. In addition to serving on several advisory and editorial boards, she founded the Summer School for Integrated Computational Materials Education, which is held annually.

Paul V. Braun is the Director of the Frederick Seitz Materials Research Laboratory and the Ivan Racheff Professor of Materials Science and Engineering, and Chemistry, at the University of Illinois Urbana-Champaign, USA. Prof. Braun received his B.S. from Cornell University, and his Ph.D. from the University of Illinois. Following a postdoctoral appointment at Bell Labs, he joined the faculty at Illinois. Prof. Braun serves on the editorial advisory boards of multiple journals, was a member of the DARPA Defense Science Study Group, and is on the National Academies Technical Advisory Board for the US Army Research Laboratory.

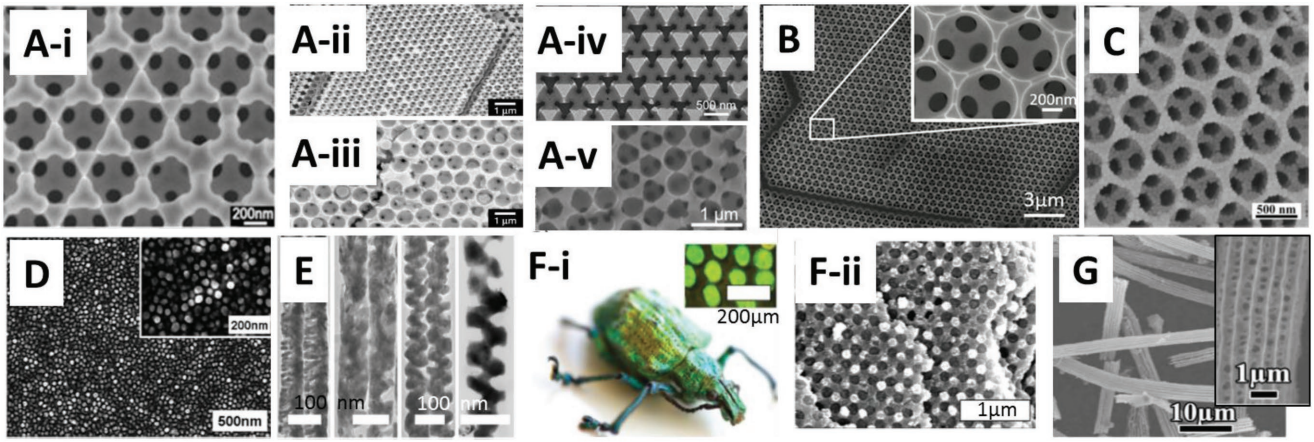

Figure 1. Examples of templated structures**.** A) Inverse opal structures of A-i) Ni, A-ii) CdSe, A-iii) CdS, A-iv) ZnO, and A-v) Cu_2O. B) Electrodeposited ReNi alloy inverse opal structure. C) Metallodielectric (Au-Silica) inverse opal films fabricated by templating colloidal crystals with gold-silica core–shell nanoparticles. D) Ultrahigh density arrays of conducting polypyrrole nanorods fabricated using electropolymerization within a porous block copolymer template. E) Nanowires of PdCu alloy electrodeposited within anodized aluminum oxide template. F) Double-imprint sol–gel biotemplating route for converting F-i) photonic scales of the weevil *L. augustus* into F-ii) high-dielectric titania replica. G) ZnO replica microtubes by the templating of *D. hyparete* butterfly wing scales. A-i) Reproduced with permission.[43] Copyright 2015, Wiley-VCH. A-ii,iii) Reproduced with permission.[33] Copyright 1999, Springer Nature. A-iv) Reproduced with permission.[35] Copyright 2017, American Chemical Society. A-v) Reproduced with permission.[34] Copyright 2014, American Chemical Society. B) Reproduced with permission.[46] Copyright 2017, Royal Society of Chemistry. C) Reproduced with permission.[47] Copyright 2002, Wiley-VCH. D) Reproduced with permission.[36] Copyright 2008, American Chemical Society. E) Reproduced under the terms of the CC-BY-NC-ND 3.0 license.[50] Copyright 2014, Springer Nature. F) Reproduced with permission.[37] Copyright 2009, Wiley-VCH. G) Reproduced with permission.[38] Copyright 2006, IOP Publishing.

an alloy, ReNi alloy inverse opals were formed by alloy electrodeposition into an opal template, with the result being a well ordered metallic foam (Figure 1B) with exceptional thermal stability, mechanical strength, and hardness relative to previously reported inverse opals.[46] These structures have been studied as thermal emitters for thermophotovoltaic devices.

Templating has also been used to direct self-assembly of materials including nanoparticles and conducting polymers. For example, gold-silica core–shell nanoparticles were assembled into an inverse opal structure using an opal template (Figure 1C).[47] These gold-silica core–shell nanoparticle-based inverse opal films showed distinct reflectances originating from the photonic crystal structure and the metallodielectric nanoparticles. In another work, highly dense arrays of a conducting polymer, polypyrrole, were grown using electropolymerization in the nanoholes of a self-assembled polystyrene-block-polymethylmethacrylate (PS-b-PMMA) block copolymer template in which PMMA was etched out.[36] After completely removing the block-copolymer scaffold, self-supported arrays of conducting polypyrrole rods oriented normal to the substrate surface were obtained (Figure 1D).

Along with colloids and block copolymers, the self-assembled structure present in anodized aluminum oxide (AAO) has also been explored as a functional template.[48,49] In one example, a PdCu alloy was electrodeposited within a nanoporous AAO template.[50] After etching away the template, PdCu alloy nanowires with a shape of the AAO template channels were obtained. Partial chemical etching of the copper from the PdCu alloy enabled modification of these superlattice PdCu nanowires to form random-chapped, random-gapped, screw-threaded, and spiral-shaped nanowires (Figure 1E).[50] These nanowires showed better stability than the pure Pd nanowires, and faster response and recovery times than pure Pd nanowires when used as hydrogen sensors.[50]

Biological structures can also be used as templates to create unique structures.[51] Some of the vibrant colors found in biological systems are known to arise from periodic structures, which strongly interact with visible light.[51] It has been shown that some of the intricate biological frameworks that color the organism can also be used as templates for synthetic structures.[37,38] As seen in Figure 1F-i, the green color in weevil *Lamprocyphus augustus* (*L. augustus*) arises from its biopolymeric exoskeleton scales arranged in a complex diamond-based photonic crystal lattice and selectively arranged single-crystal domains.[37] These diamond-based photonic lattices have been used as structural templates for silica or titania (Figure 1F-ii). The high-dielectric-constant titania photonic crystal showed reflectance peaks around 570 nm corresponding to the expected stopbands of its diamond-based photonic crystal structure. In a similar work, complex microstructures of ZnO were synthesized using the butterfly-wing scales of *Delias hyparete* (*D. hyparete*) (Figure 1G) as templates.[38] The ZnO replica microtubes formed had porous walls resembling the scales on the wings of the butterfly.

3. Template-Directed Assembly: Emergence of New Structures

In the examples discussed above, the template merely served as a porous host, which was filled or partially filled with a second phase material. A potentially more interesting case is when the template leads to the emergence of additional symmetry elements in the templated material structure not directly present in the template. It is also interesting to consider if a template can significantly control or reduce the density of structural defects in a self-organizing material. As discussed,

self-organization has been widely used to form large-area photonic crystals, however, these structures always contain point, line, and other defects.[52–55] To reduce defect density, it has been shown that colloidal crystals can be epitaxially grown on patterned substrates.[56] Use of a patterned substrate to direct assembly has proven promising for reducing the defect density of other self-organizing systems too.[11,57–61] Pioneering examples of template-directed assembly of block copolymers, molecular systems, nanoparticles, and spontaneously phase-separating alloys are reviewed in this section. The template-directed assembly can be based on topographic patterns, chemical surface modifications, and confinement effects.[11,62] Here, we survey results for a variety of material chemistries, showing the versatility of this technique and applicability to the field of optics. Such template-based processes have the advantage of scalability and controlled placement of materials since they build on well-studied lithographic patterning strategies that offer nanometer to micrometer precision.

The template-directed assembly of block copolymers has been extensively studied.[61,63–67] In one example, a chemically modified nanopatterned (by extreme UV interferometric lithography) surface was used to direct the assembly of a lamellae-forming diblock copolymer, PS-b-PMMA.[63] The PS domains preferred the unmodified regions of the surface whereas the PMMA domains preferentially wetted the chemically modified surfaces of the patterned surface (**Figure 2**A). Such epitaxy directed self-assembly of block copolymers is not limited to the use of lamellae-forming PS-b-PMMA, but is also applicable to cylinder forming block copolymers. This was demonstrated

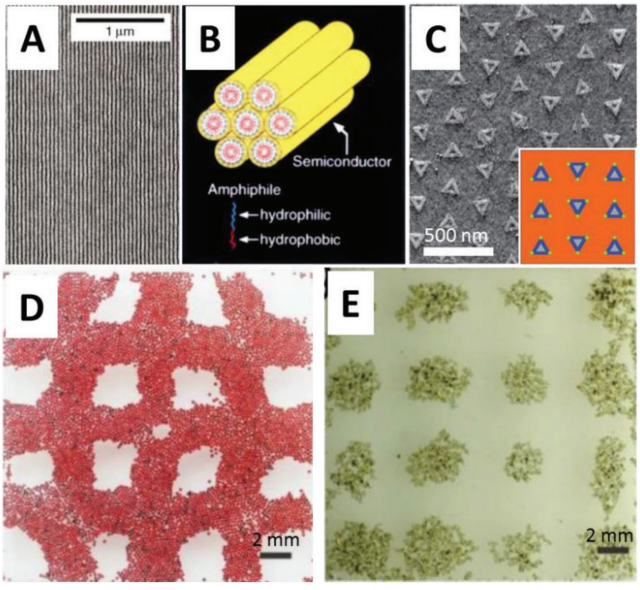

Figure 2. Template-driven self-assembly and emergence of new structures. A) Directed self-assembly of block copolymers printed onto a chemically patterned substrate. Reproduced with permission.[63] Copyright 2003, Springer Nature. B) Semiconducting superlattices templated by molecular assemblies. Reproduced with permission.[69] Copyright 1996, Springer Nature. C) Arrays of gold nanoparticles directed by lithographically confined DNA origami. Reproduced with permission.[59] Copyright 2009, Springer Nature. D,E) Microscale assembly of copper–zinc powder and polystyrene divinylbenzene beads, respectively, directed by a liquid-based template. Reproduced with permission.[57] Copyright 2014, Wiley-VCH.

with the polystyrene-block-polyisoprene diblock copolymer that was directionally solidified on a topographically patterned substrate.[64] The topography of the patterned substrate provided a sufficient bias to control the long-range order of the block copolymer. Such template-directed block copolymer assemblies have been proposed for magnetic, data storage, and photonics applications.[63–66]

Template-directed assembly of molecules, DNA, and nanoparticles can also give rise to micro and nanoscale structures with promising optical responses. Molecular assembly is an attractive route to obtain nanostructured composites since the molecules can be chemically designed to provide a favorable environment for the growth of specific materials.[62,68] In one study, preordered self-assembled amphiphiles were used as sites for the precipitation of inorganic semiconductors (e.g., CdS) forming semiconductor superlattices that match the symmetry and periodicity of the initial self-assembled amphiphiles (Figure 2B).[69] Exceptionally fine control over particle assembly can be achieved by combining bottom-up self-assembly of DNA scaffolds and directed assembly of nanoscale materials on these scaffolds.[70–73] When the DNA assembly is precisely controlled by using a patterned surface, DNA origami can be a powerful tool, for example, by dictating the arrangement of sub 10 nm components (gold nanoparticles) over large scale areas (Figure 2C).[59] In another work, by guiding the alignment of liquid crystals via topographic and chemical patterns, the defect structure of the liquid crystals was then used to trap colloidal particles, leading to their patterned arrangement.[74]

In a unique approach, liquid surfaces containing standing waves have been used as large-area reconfigurable templates for the assembly of microscale materials.[57] This has been demonstrated for a large range of periodicity, from a few microns up to millimeters, and a variety of material chemistries.[57] Particles on the liquid surface organize through a combination of the forces of surface tension, buoyancy, and gravity. Materials selectively arrange into patterns at the nodal or antinodal regions of the standing wave. For instance, copper–zinc powder assembles in the antinodal regions whereas polystyrene divinylbenzene beads assemble in the nodal regions (Figure 2D,E), forming complimentary patterns consisting of two rather different materials.[57] In this approach, many symmetries of standing waves can be formed on liquid surfaces, and the surface patterns can be rapidly reconfigured.

It is important to remember that obtaining novel optical properties over visible to near-IR wavelengths of light requires control of structure from the nanometer to micrometer scale. While molecular, nanoparticle, and DNA-based self-assembly processes are effective for controlling structure at the nanometer scale, they are not well suited to control structure over longer length scales. This is where the emerging methods of eutectic solidification and spinodal decomposition of optically active materials appear particularly promising. Both spinodal decomposition and eutectic solidification offer control of constituent structural features from the nanometer-scale to micron-scale, as well as the choice of a variety of materials with interesting optical properties. During these diffusion-dependent phase-separation processes, the initial material separates into two distinct phases.

A variety of material combinations undergo spinodal decomposition, a process in which a thermodynamically

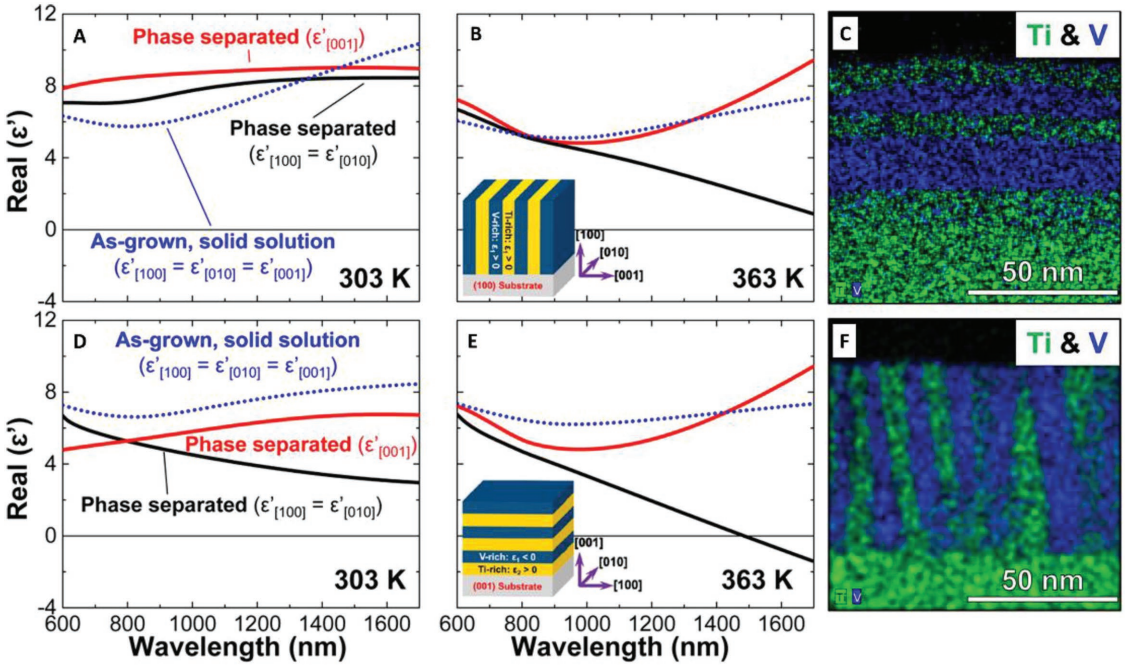

Figure 3. Nanostructured and tunable metamaterials via spinodal decomposition. Optical dielectric constant and high-resolution elemental mapping for A–C) (100)- and D–F) (001)-oriented heterostructures. Reproduced with permission.[84] Copyright 2016, American Chemical Society.

unstable system phase separates spontaneously without nucleation.[75–79] In this process, phase separation occurs through diffusion in the direction of increasing concentration due to the second derivative of the free energy with respect to composition having a negative sign. Spinodal decomposition has been studied in many materials systems, including Al–Zn,[80] Au–Pt,[81] Cu–Ti,[82] VO_2–TiO_2,[83] SiO_2–TiO_2,[83] SiO_2–ZnO.[83] These material systems have a potential to exhibit unique optical properties arising from the combination of the two constituent phases. Further details on spinodal decomposition can be found in other works.[75–79] The VO_2–TiO_2 material system is of interest as an optical material since the component oxides have distinct contrasting optical properties. Additionally, the temperature dependent metal-to-insulator transition of VO_2 provides a mechanism for optical tuning. Using pulsed-laser deposition, epitaxial and single-phase solid solution thin-films of $V_{0.6}Ti_{0.4}O_2$ were grown on rutile TiO_2 (001)- and (100)-oriented single-crystal substrates.[84] Upon annealing, this solid solution decomposed into phase-separated VO_2–TiO_2 nanocomposite structures. As shown in **Figure 3**, the epitaxially grown thin films formed layers aligned either horizontally or vertically depending on the orientation of the underlying single-crystal substrates. These (001)- and (100)-oriented heterostructures exhibited unique optical behavior in the near-IR wavelength regime. With increasing temperature, the VO_2 became metallic, and the optical dielectric constant of the (001)-oriented heterostructures transitioned from positive to negative values, further enhancing the uniaxial anisotropy of the optical response. Thus, the orientation change combined with the metal-to-insulator transition of the VO_2 phase demonstrated the temperature-tunable optical transformation of the material from a nonhyperbolic to a hyperbolic metamaterial.[84]

Similar to spinodal decomposition, eutectic solidification provides phase-separated micro and nanoscale structures whose periodicities can be easily tuned on the order of the wavelength of light, from the visible to infrared regime. Details on the solidification of eutectic materials and their potential optical applications are first discussed in Section 4. Then, how templates can be used to control and enhance the microstructure of eutectic optical materials is surveyed in Section 5.

4. Directionally Solidified Eutectics as Advanced Optical Materials

Eutectic material systems have two or more chemical components for which a liquid and two or more solid phases coexist in equilibrium at the eutectic temperature (T_E) and composition (C_E);[14,17,26] the point (C_E, T_E) on a phase diagram is called the eutectic point. A typical binary eutectic phase diagram for a two-component system (with chemical species A and B), is shown in **Figure 4**A. During solidification of such a eutectic melt, the liquid phase-separates into two distinct solid phases α and β. The simultaneously solidifying phases generally organize into simple motifs consisting of alternating layers (lamellar morphology) or fibrous structures (rod morphology) (Figure 4B); however, complex structures, such as spiral or broken lamellar, globular, elongated rods, or even structures with similarities to split-ring-resonators, are also possible (Figure 4C).[14]

The microstructure of a eutectic material is dependent on factors including composition, atomic or ionic diffusivity, interfacial energies, thermal conductivity, and latent heat of fusion of the individual components.[14,17,87–90] Another important parameter is the rate of solidification, defined as the velocity of the solidification front, v. Depending on the solidification

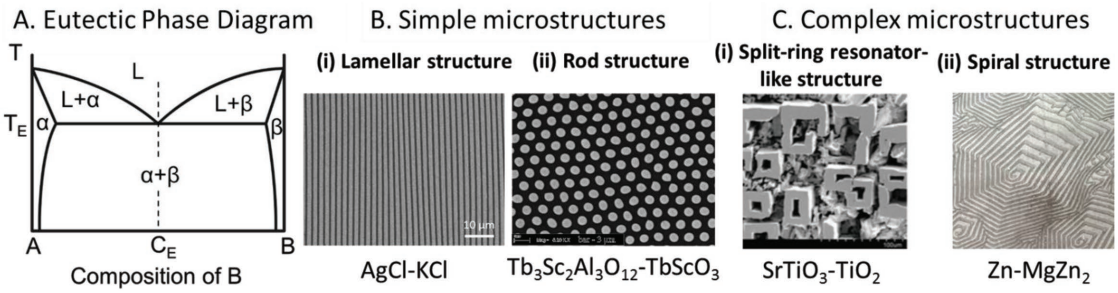

Figure 4. Directionally solidified eutectics. A) Schematic of a typical binary eutectic phase diagram. Examples of simple microstructures: B-i) Lamellar structure (AgCl–KCl eutectic) and B-ii) rod structure ($Tb_3Sc_2Al_3O_{12}$–$TbScO_3$ eutectic), reproduced with permission.[85] Copyright 2006, American Chemical Society. Examples of complex microstructures: C-i) Split-ring resonator-like structure ($SrTiO_3$–TiO_2 eutectic), reproduced with permission.[86] Copyright 2010, Wiley-VCH. C-ii) Spiral structure (Zn–$MgZn_2$ eutectic, imaged at 1200× magnification).[87] Used with permission of The Minerals, Metals & Materials Society.

technique, v can be controlled by external parameters, e.g., the temperature gradient in the furnace, sample draw rates through the furnace, and printing speeds.[87,91–94] The laser floating zone method,[95] the micropulling down approach,[85,96] the Czochralski method,[97] the Bridgman furnace,[92,98] and direct-ink writing,[94] are examples of methods utilized for the directional solidification of eutectics. The rate of solidification controls the feature size (layer widths, particle or fiber diameter) and the characteristic spacing (λ) of the periodic structures. Under steady-state conditions of eutectic growth, $\lambda^2 v$ is constant for the given material system, thus fast rates of heat removal lead to small characteristic spacing and vice versa.[88] This characteristic spacing control can be effective over a wide range, from tens of nanometers to hundreds of microns, without changing material systems.[99] The constituent materials of the eutectic can be chosen from many material types, including metals, organics, salts, ceramics, semiconductors, and polymers.[100–102]

To date, the optical properties of only a handful of eutectic systems have been studied, leaving a vast number of material systems unexplored. Given that eutectics containing both dielectric and metallic phases can be organized into a diverse set of microstructures, there is a potential for discoveries of unique optical metamaterials, thermally anisotropic materials, and magnetoresistive materials.[103,104] Eutectics generally solidify in the form of monoliths with good bonding between their constituent phases.[14,87,91,92] Moreover, the interface between the two phases is generally sharp and therefore the light scattering loss from interfacial roughness and mismatch defects are minimized. Refractive index profiles that resemble 1D and 2D photonic crystals, can be realized by regular lamellar and rod eutectic structures, respectively.[1] Although eutectic structures have been known for nearly a century, only limited examples of their optical properties can be found in the literature (**Table 1**).

Alternating layers, with sub-micron widths and different refractive index in lamellar structures (of Al_2Cu–Al and AgCl–KCl eutectic) have been used as 1D diffraction gratings in the visible light wavelength range.[94,105] At wavelengths above the periodicity of the lamellae, the alternating lamellar layers could be utilized as wire-grid polarizers as demonstrated for InSb-Sb and Ga–In eutectic systems in the mid-IR to sub-THz wavelength regime.[106,107] These lamellar structures resemble 1D photonic crystals, and because they consist of alternating layers of materials with different dielectric constants, they exhibit a photonic bandgap. As exhibited in salt eutectics, AgCl–KCl,[93] and AgCl–$CsAgCl_2$,[108] the photonic bandgap can be in the visible to near-IR regime. Similar eutectic structures have also been used as broadband planar optical waveplates (as in calcia stabilized zirconia, $CaZrO_3$, eutectic).[109] 2D photonic crystals with bandgaps in the visible to near-IR wavelength range are produced when the eutectic organizes into a rod structure (as in AgCl–$CsAgCl_2$,[108] CaF_2–MgO,[98] NaCl–LiF,[110] and MgF_2–MgO[111] eutectic). The rod structures of some of the alkali halide binary salt eutectics have also been demonstrated for light guiding in phase-separated scintillators (one of the two phases is selectively doped with metallic or rare-earth elements).[112] Recently, fluoride-containing eutectic salts with rod structures (of KCl–LiF and NaCl–LiF eutectic) have been studied for their polaritonic properties as they can behave as metamaterial waveguides with near-zero permittivity (so-called epsilon-near-zero metamaterials) or exhibit absorption-induced transparency.[113,114]

The phase-separated composites have also been used for their material properties that are not dependent on possessing a well-ordered periodic microstructure. A broadband visible to mid-IR optical quality glass was obtained using a $CaSiO_3$–$Ca_3(PO_4)_2$ eutectic.[115] A polymer based eutectic consisting of poly(3-hexylthiophene) and [6,6]-phenyl C_{61}-butyric acid methyl ester was successfully incorporated as the photocurrent generator in a bulk-heterojunction photovoltaic device.[116] The organic acid eutectic system of 3-nitrobenzoic acid and 3,5-dinitrobenzoic acid has shown enhanced second harmonic generation in the visible to near-IR regime.[117] Finally, the combination of a metal–dielectric eutectic system composed of Ag and Bi_2O_3 was recently explored for its localized surface plasmon resonance properties. Upon doping the oxide with rare-earth elements, this system exhibited plasmon enhanced photoluminescence.[118]

4.1. Challenges and Opportunities for Eutectic Optical Materials

In the examples discussed so far, the optical properties of the eutectic systems are derived from the symmetry, characteristic spacing (λ), and degree of perfection of the microstructure along with the properties of the constituent materials. A

Table 1. Experimentally observed optical functionality in directionally solidified eutectic systems.

Optical functionality	Eutectic material system	Wavelength regime	References
Diffraction grating	Al_2Cu–Al	Visible	[105]
	AgCl–KCl		[94]
Wire-grid polarizer	InSb–Sb	Mid-IR	[106]
	Ga–In	Sub-THz	[107]
Photonic bandgap crystals	AgCl–KCl	Visible to near-IR	[93]
	AgCl–$CsAgCl_2$		[108]
Planar optical waveguide	Calcia-stabilized zirconia $CaZrO_3$	Visible to mid-IR	[109]
Fiber optic waveguide	CaF_2–MgO	Visible to near-IR	[98]
	NaCl–LiF		[110]
Fiber optic faceplate	MgF_2–MgO	Visible to near-IR	[111]
Phase-separated scintillators with light guiding	CsI–NaCl, CsI–RbF	Visible to near-IR	[112]
	RbI–NaCl, CsBr–NaCl		
	CsBr–NaF, RbCl–NaCl		
Absorption-induced transparency and localized enhanced optical transmission	NaCl–LiF	Mid-IR to THz	[113]
	KCl–LiF		
Epsilon-near-zero metamaterial waveguide	KCl–LiF	THz	[114]
Optical quality glass	$CaSiO_3$–$Ca_3(PO_4)_2$	Visible to mid-IR	[115]
Photocurrent generator in photovoltaic devices	Poly(3-hexylthiophene)–[6,6]-phenyl C_{61}-butyric acid methyl ester	Visible	[116]
Enhanced second harmonic generation	3-nitrobenzoic acid – 3,5-dinitrobenzoic acid	Visible to near-IR	[117]
Plasmonics	Bi_2O_3–Ag	Visible	[118]

significant challenge is how to synthesize large-area ordered and defect-free eutectic structures. Typically, good order is only observed over submillimeter length scales, limiting the potential applications to those that either only require small samples, or are tolerant of disorder in the structures. Another challenge is the limited number of microstructure types that can be realized via eutectic solidification while retaining a high degree of order. As an example of possible approaches, recently an organic eutectic was solidified with a rotational solidification method, generating materials with chiral and spiral morphologies, which resemble structures that could function as a hyperlens.[119] We will discuss in Section 5 how this limitation in the available microstructures, as well as the general absence of long-range order in solidified eutectic systems, can possibly be overcome by the use of templates.

There is a vast library of eutectic materials that are yet to be explored for their optical properties,[120] as well as a wide range of processing conditions that can be applied. The number of variables here indicates a phase space that cannot be efficiently studied through experiments alone, which is why the application of simulation and theory is critical to explore even simple systems. Additional complications arise when studying complex (or anomalous) eutectics, such as Al–Ge or Al–Si,[121,122] as the structure of these systems are highly dependent on the growth mechanisms of the individual phases.[17] These metal-dielectric systems are particularly interesting for metamaterial applications, which require one phase of the system to have a metallic character. To date, the nature of the solidification in these metal-dielectric eutectic systems has made it difficult to achieve precise control over the orientation and long-range order of the solidifying structure, as well as its computational investigation.[123–126]

Another promising approach is doping the eutectic phases with rare-earth elements or metallic nanoparticles to introduce optical gain or loss, respectively, which could lead to various exceptional optical phenomena including superprism effects, supercollimation, and arbitrary polarization control in birefringent metamaterials.[127–130]

It is clear that the microstructure present in solidified eutectics can result in materials with significant potential for photonic applications. However, to fully realize the potential of eutectic solidification, and as will be discussed later in the review, it is crucial to make use of quantitative models that can predict the microstructures formed by eutectic solidification. Here, we discuss an example of such models based on phase-field modeling.

4.2. Phase-Field Modeling of Eutectic Microstructure Evolution

Predicting the microstructure of self-organizing systems is challenging even when the underlying physics is well understood. With the growth of computational resources and improvements in computational capabilities, numerical simulation has become a practical approach for solving complex problems such as this. Simulations of microstructural evolution have been conducted utilizing many different methods,[131–149] spanning a wide range of time and length scales.

An important element of modeling multiphase and composite systems is how to describe interfaces. There are two approaches for treating interfaces mathematically. One approach is known

as the sharp interface model that considers interfaces between phases as surfaces with zero thickness. Simulations based on this approach follow the positions of the interfaces at every time step. Boundary conditions are imposed on these sharp interfaces, which may have complex morphologies. The level set method,[137] the boundary integral method,[150] and the enthalpy method[141] have been developed based on sharp interface models to simulate eutectic solidification. Another approach, the so-called diffuse interface model, represents interfaces with a field defined in three dimensions, which includes a transition region with a finite thickness near phase boundaries.[151] The field varies smoothly from one phase to another, and therefore appears diffuse, leading to its name. The interfacial locations are determined from this field, rather than explicitly tracked. The phase-field model is one type of diffuse interface model developed for simulating phase transformations and microstructural evolution because of its ability to take into account both the thermodynamics and kinetics of materials.

Phase-field models represent phases with a field called as an order parameter. An order parameter may correspond to the concentration of a chemical species, which is distinct in different phases, or represent the degree of order/disorder at the atomic level (e.g., crystalline solid vs liquid). The order parameter takes a constant value in the bulk regions of a phase, transitioning smoothly between these values at the interfaces between phases with a finite thickness. The temporal change of the order parameter implicitly captures the motion of interfaces without explicit tracking. The thickness of the interface in a phase-field model is a numerical input parameter and is typically chosen to be much larger than the physical interfacial thickness to increase computational efficiency without affecting the dynamics when the interfacial thickness is taken to be sufficiently small compared to characteristic length scales in the system.[152,153]

The temporal evolution of the order parameter is driven toward configurations that decrease the total free energy of the system. The total free energy, F is defined as the integral of the local free energy density, f, in space

$$F = \int_V f \, \mathrm{d}V \tag{1}$$

The most basic form of the free energy density consists of two terms: bulk free energy density describing the thermodynamics of the material and energy density that penalizes gradient in the order parameter. These two terms together describe the energetics of the system, including the interfacial energy. An example of f can be given by

$$f = w\phi^2(1-\phi)^2 + \frac{\epsilon^2}{2}(\nabla\phi)^2 \tag{2}$$

where the bulk free energy is modeled with a double-well function, and w and ε are the double-well height and gradient energy coefficient, respectively. The term $w\phi^2(1-\phi)^2$ is the bulk free energy that induces phase separation due to the energy minima at bulk phase values of $\phi = 0$ and $\phi = 1$. A more realistic model includes dependences on other variables, such as temperature in solidification modeling. The other term, $\frac{\epsilon^2}{2}(\nabla\phi)^2$, provides an energy penalty for large gradients in the order parameter, resulting in interfaces with a finite thickness. Additional free energy density terms can be added to capture the underlying physics of a system, such as elastic strain energy. Based on the constructed total free energy, the rate of change of the order parameter at each point, $\partial\phi/\partial t$, is given by two types of equations. For a conserved order parameter (e.g., a concentration field), the Cahn–Hilliard equation,[154] which results from mass conservation with a flux driven by chemical potential gradient, applies

$$\frac{\partial\phi}{\partial t} = \nabla\cdot\left[M\nabla\left(\frac{\delta F}{\delta\phi}\right)\right] \tag{3}$$

where M is a mobility associated with the conserved order parameter and $\delta F/\delta\phi$ is the variational derivative of F,[155] which is an infinitesimal change of F corresponding to an infinitesimal change of ϕ. For a nonconserved order parameter (e.g., a field representing the degree of atomic-level order/disorder), the Allen–Cahn equation is applied[156]

$$\frac{\partial\phi}{\partial t} = -L\nabla\left(\frac{\delta F}{\delta\phi}\right) \tag{4}$$

where L is a mobility associated with the nonconserved order parameter.

Phase-field models have an advantage of easier numerical implementation compared to most sharp interface models. Here, boundary conditions do not need to be imposed on the interfaces, which often have complex morphologies. This enables the use of the finite difference method,[157] which is a straightforward numerical approach for solving partial differential equations. The validity of phase-field models can be assessed by examining the sharp interface asymptotics for the phase-field model,[152,153,158,159] and by comparing the phase-field simulation results to the sharp interface models.[160,161]

Phase-field models of eutectic solidification have been developed[162–166] based on the quantitative phase-field models of solidification.[152,153,167–169] Early phase-field models for eutectic solidification were demonstrated for binary eutectics but were not computationally efficient because fine spatial resolutions were required for resolving composition gradients and their evolution within the interface.[170–173] Multiphase-field models enabled examination of three or more phases.[162,163] These models were further developed to improve accuracy and computational efficiency by mitigating a diffuse interface artifact (i.e., solute trapping) and have been validated against the Jackson–Hunt theory.[88,164–166]

Many aspects of microstructural formations in eutectic solidification have been studied by using phase-field models. Phase-field simulations of eutectic colony formation[174] and lamellar stability during solidification[175–178] have provided insights into eutectic morphological evolution. Phase-field simulation results confirmed the existence of a eutectic colony structure, which has shorter-range (i.e., lamellae) and longer-range (i.e., eutectic colony cell) periodicity,[174] which were predicted by the long-range instability in a linear stability analysis.[179] The overstability condition of small lamellar spacing was studied by phase-field modeling and experiments revealing transverse movement of phase triple junctions not considered in the

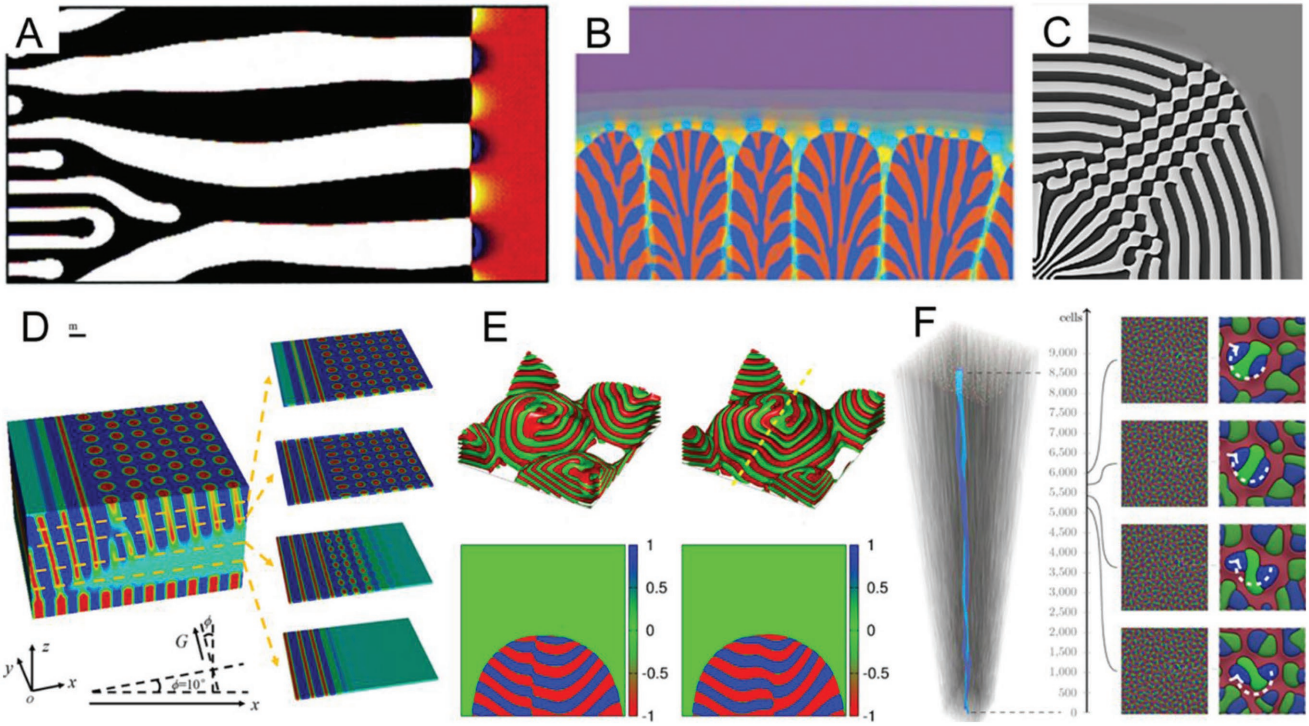

Figure 5. Various eutectic pattern formations captured by phase-field modeling. A) Lamellar structure formation during directional solidification. Reproduced with permission.[162] Copyright 2000, Elsevier. B) Eutectic colony formation during directional solidification. Reproduced with permission.[174] Copyright 2002, American Physical Society. C) Lamellar breakdown during isothermal solidification under thermal noise and continuous nucleation. Reproduced with permission.[176] Copyright 2007, Springer Nature. D) Lamellar-to-rod structure transition during directional solidification due to change in the temperature gradient direction. Reproduced with permission.[184] Copyright 2017, AIP Publishing LLC. E) Spiral eutectic colony pattern formation due to anisotropy in interfacial energies. Reproduced with permission.[183] Copyright 2017, Elsevier. F) Spiral growth of rods during directional solidification of a ternary eutectic. Reproduced with permission.[188] Copyright 2016, Elsevier.

derivation of the Jackson–Hunt theory.[175] Phase-field simulations of the continuous nucleation of solid phases during eutectic solidification were performed and revealed that the nucleation can suppress instabilities of interfaces between a single solid phase and the eutectic liquid.[176] Also, the formation of a zig–zag type lamellar structure was found and analyzed.[177] Subsequently, the stability of structural defects in lamellar and other unique periodic microstructures not considered in the Jackson–Hunt theory were revealed.[178] The effects of planar geometric confinement on the resulting eutectic microstructures were examined, and several microstructural features rarely seen in experiments were discovered.[180,181] As in all multiphase materials, interfacial energies play a key role in eutectic microstructure evolution, and thus the effects of anisotropy in interfacial energy were studied.[182,183] The results showed a wide variety of morphological patterns, such as spiral eutectic colony structure, due to interfacial energy anisotropy.[182,183] The effects of the temperature profile were investigated, and a lamellar-to-rod microstructural transition was found in the directional solidification of the eutectic with the temperature gradient direction transverse to the solidification direction.[184] Ternary eutectic systems, in which three solid phases form simultaneously, were studied for lamellar growth in two dimensions[185] and spiral growth of two-phase rods embedded in a matrix phase in three dimensions.[186–188] Eutectic phase-field models have been employed to simulate many different types of eutectic material systems, including metals and ionic compounds. **Figure 5** shows various types of eutectic microstructures (including lamellar, colony, rod, and spiral structures) that have been successfully simulated with phase-field models.

5. Template-Directed Solidification of Eutectic Materials

Template-directed assembly has already shown potential to improve the order of self-organizing systems based on block copolymers, amphiphilic molecules, spinodal decomposition, and nanoparticles, for applications ranging from data storage to optics (see Section 3). Here, we discuss how this concept is showing promise for controlling the self-organization of eutectic materials to generate microstructures that could have potential optical functionalities. This template-directed solidification could also lead to the emergence of new structures that are not present in either the template or the native eutectic structure. As the variables associated with a template's geometry further broaden an already large phase space, simulation methods would be key to making efficient progress in understanding the microstructural evolution and the development of templates.

In a template-directed process, the resultant microstructure depends upon specific interactions of the template with

the solidifying eutectic material. Using a template, there is the potential of forming new photonic crystal and optical metamaterial architectures, as well as the possibility that structures with long-range order can be realized. This calls for designing architectures focused toward novel 2D and 3D patterns with precise placement of the solidifying eutectic. Such a precise control requires fundamental understanding of the concepts of eutectic–eutectic and eutectic–template interactions.

State-of-the-art tools like lithography and surface functionalization can be used to design a template matrix with a patterned topography and surface chemistry. With this, the effects of confinement and the interaction between the template pattern and the solidifying eutectic (for surface-selective nucleation) can be combined to tailor the assembly of the phase-separating components. As reviewed in Sections 2 and 3, the combination of top-down lithography and bottom-up assembly of materials gives opportunities to fabricate large-area, scalable optical materials, and widen the scope of constituent structures and materials.

Some work has already been done to show the effect of templates on eutectic solidification and it has long been known that a template can be used to control the resulting functionality of the system. For example, $LiBH_4$, which has been explored as a hydrogen storage material given its high hydrogen content of 18.5 wt%, demonstrated enhanced hydrogen storage performance when confined within nano and microporous templates. To infiltrate $LiBH_4$ into porous materials, it was helpful to form eutectic mixtures, as this decreases the melting point and thus the required temperatures for melt infiltration.[189–191] In one case, the eutectic $LiBH_4$–$Ca(BH_4)_2$ was successfully infiltrated into mesoporous carbon, and the positive effects of nanoconfinement were observed through the enhanced hydrogen desorption and absorption properties, improving the hydrogen storage performance of the device.[189]

Perhaps not surprisingly, it has been observed that the nanoconfinement of eutectic materials within a porous template leads to slight modifications in the phase diagram and melting characteristics as interaction between the eutectic melt and the template surface changes the overall thermodynamics of the system.[192,193] A detailed understanding of these interactions is crucial in designing templates, as it is these interactions, coupled with the reduced dimensions of the environment that determine much of the effects of confinement on the resultant eutectic microstructure.[193] Note that the overall shape of the phase diagram of the confined mixture does not change; however, there is some shift in the melting temperatures and concentrations with respect to the bulk mixtures. It has been demonstrated in some nanoscale confined binary organic eutectic mixtures (e.g., $C_6H_4Br_2$–CCl_4) that the melting temperature of the mixtures decreases relative to the bulk eutectic when the melt–wall interactions are weaker than the melt–melt interaction as seen in the case of infiltrated silica glasses.[193] However, in the case of infiltrated mesoporous carbon where the melt–wall interactions are stronger than the melt–melt interactions, the melting temperature increases. Thus, it is critical to take into account the thermodynamic effects of the interaction of the eutectic and template surface that can modify the conditions of eutectic solidification.

5.1. Effects of the Shape of the Solidification Front

A few cases of template-directed solidification of eutectics have been studied in literature, as reviewed below, wherein factors affecting the solidification process and the final structure are either the template-dictated shape of the solidification front or confinement within the patterned template. The periodicity of the eutectic (λ) is primarily determined by the solidification front velocity (v). Depending on the manner of heat removal from the eutectic melt and the design or composition of the container/template, the solidification front can assume different shapes and orientations. Hence, the template design and template composition are both crucial in determining the shape of the solidification front for a given method.

As one of the initial examples of template-directed solidification of eutectics, it was demonstrated that by forcing the solidification front to curve, either by adjusting the heat-flow pattern or by blocking the eutectic growth with a physical obstacle, the lamellar structures of some eutectics (Pb–Cd, Sn–Cd, and Cd–Zn) transition into rod structures.[194] Over the range of the applied growth rates, the Pb–Cd eutectic always formed an ordered lamellar structure in the absence of obstacles. To produce a curved solidification front, the eutectic was directionally solidified in a graphite boat containing a graphite inset as shown in **Figure 6**. In this setup, the metal eutectic solidified with a planar solidification front until the front reached the sharp edge of the graphite inset. At the edge, the solidification front curved as it grew around and past the inset obstacle without significant change to the growth rate. However,

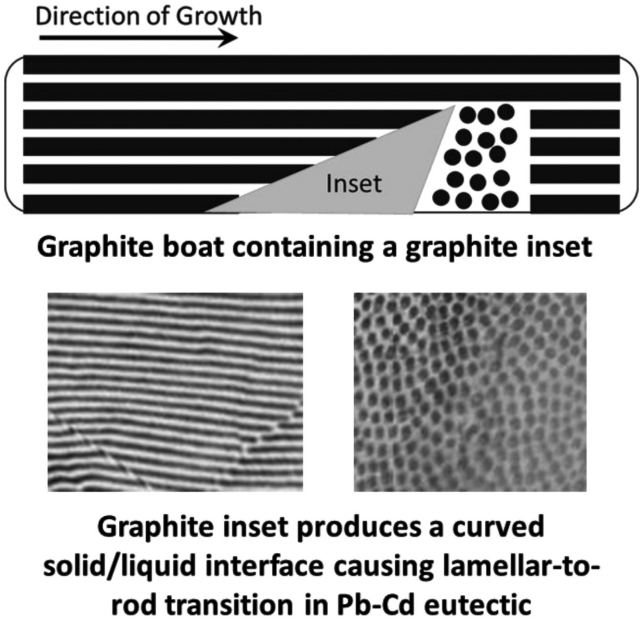

Figure 6. Modifying the shape of the eutectic solidification front by introducing an obstacle in its solidification path: Pb–Cd eutectic shows a lamellar structure; however, when its solidification path is modified by a graphite inset, the solidification front curves around the inset, causing a lamellar-to-rod transition in the eutectic (imaged at 1125× magnification). Reprinted with permission of Taylor & Francis Ltd., on behalf of The Institute of Materials, Minerals and Mining.[194] Copyright 1963, The Institute of Materials, Minerals, and Mining.

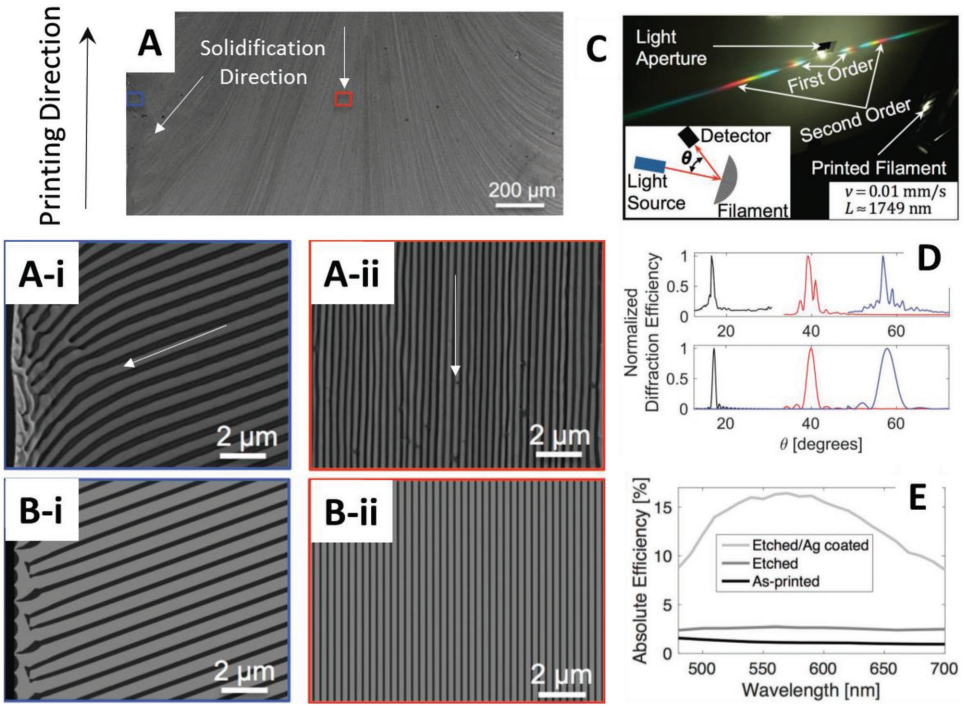

Figure 7. Printed eutectic filaments as diffraction gratings: AgCl–KCl eutectic printed using the direct-ink-writing technique. The center of the printed filament shows straight lamellae aligned along the printing direction. At the edges of the filament, the lamellae curve outward as confirmed by the phase-field modeling. Reproduced with permission.[94] Copyright 2016, Wiley-VCH.

the lamellae broke down into rod structures as the growth direction curved and pointed out of the plane of the initial growing lamellae. The rods did not extend far from the edge of the graphite inset, rather there was a rapid transition back to lamellae, suggesting that the rods must be growing under unstable conditions. Thus, it was concluded that the sudden change in either the direction of the solidification or the curvature of the solidification front caused by the template led to this unique observation of morphological changes.[194]

The shape of the solidification front is also affected by the heat-flow pattern during the directional solidification of the eutectic. This is a crucial parameter that determines the overall alignment of the eutectic structures. This heat-flow dependence was demonstrated in the high-operating-temperature direct-ink writing of a binary salt eutectic, AgCl–KCl.[94] The salt eutectic had an excellent overall alignment of its lamellae along the printing direction as shown in **Figure 7**A, however, along the edges of the printed filament, the lamellae curved.[94] The additional heat loss from the edges of the printed eutectic to the cold ambient air would result in the change in the solidification front direction, which was hypothesized to be the cause of the observed curved lamellae. A simulation was performed based on the experimental setup and the heat transfer parameters of the eutectic mixture (Figure 7B), which matched the experimental observation.[94] In addition, the simulation indicated that the printing head imposed a curved isotherm boundary, leading to a small variation in the values of the lamellar spacing from the edge of the printed filament to its center.[94] In fact, it should be possible to reshape the printing head in such a way that the edge effect can be amplified to vary the lamellar orientation across the entire filament, for example, to obtain fully curved lamellae. Such curved lamellar structures could exhibit inherent chirality from its structure, similar to the case of rotational solidification that produced a spiral eutectic structure.[119]

The high-operating-temperature direct-ink printing method described above provided precise control over the lamellar spacing by adjusting the printing velocity, and therefore these filaments could be used as diffraction gratings in the visible to near-IR wavelength regime (Figure 7C).[94] Angle-dependent spectral measurements were carried out on these samples (Figure 7D), and the diffracted light was found to behave in the same manner as in model gratings, with slight variations arising due to the imperfections in the printed lamellar architecture. The diffraction efficiency from the first order peaks was increased (from <1.6% to ≈2.5%) by selectively etching the KCl phase to increase the refractive index contrast. Further enhancement of the diffraction efficiency (≈15%) was achieved by coating the AgCl layers with silver (Figure 7E), which was in good agreement with the optical simulations.[94]

Apart from the physical obstacles and the solidification conditions, templates can be fabricated such that specific heat-flow patterns can be generated. Such a template design was realized in the eight-legged 3D cage structure shown in **Figure 8**A,B.[195] These ribbon-shaped legs consisted of an air core, a Si ribbon, and a SiO_2 shell. The composite structure and the contrasting heat transfer properties of the component materials gave rise to a nonuniform heat-flow pattern. Upon cooling a molten AgCl–KCl eutectic-covered cage, solidification began at the top of the cage and proceeded down the length of the ribbons, as seen by the alignment of the AgCl–KCl eutectic lamellar structure, which is parallel to the tangent to the ribbon (Figure 8C–E).[195]

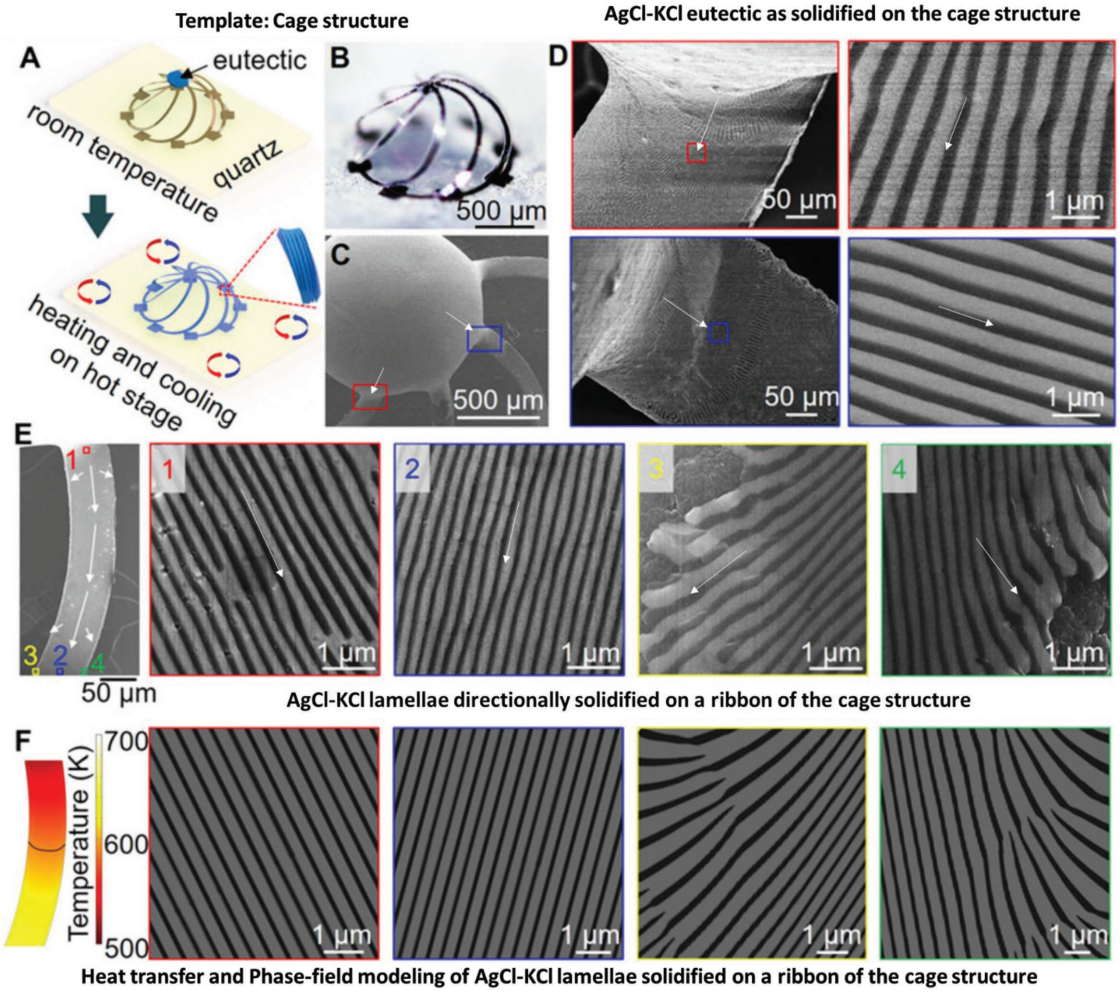

Figure 8. 3D cage structure template-directed solidification of eutectic: AgCl–KCl eutectic as solidified on a cage structure. Reproduced under the terms of the CC-BY-NC-ND 4.0 license.[195]

As calculated by heat transfer simulations for the nonuniform composite ribbon, the solidification front (which is assumed to be the isothermal surface at the eutectic temperature) had a curvature such that the solidification direction is outward at the edges of the ribbon (Figure 8F).[195] The simulated direction of solidification explains the curvature in the lamellae at the edges of the structure seen in experiment. This template manufacturing technique can create a variety of 3D shapes,[195,196] providing unique opportunities to grow template-directed eutectic materials for optical applications.

These applications show that, by controlling the shape of the solidification front via template design, novel structures of self-organizing eutectic materials can be obtained. Further studies are required to apply these concepts to form optically functional structures.

5.2. Effects of Confinement within the Template

In addition to controlling the shape of the solidification front, templates can greatly modify the microstructure of a solidifying eutectic, in particular when the template has characteristic dimensions commensurate to the characteristic spacing of the eutectic structure.[93] Templates have been used to demonstrate the effects of confinement on eutectic solidification with those ranging from 1D structures, such as capillary tubes and porous anodized aluminum oxide, to 3D structures, such as silica opals, which are further discussed below.

Optically transparent eutectic organic alloys are advantageous for studying eutectic solidification, as their transparency enables direct, in situ observation of directional solidification, which provides the details of the evolution of the solidification front and the formation of eutectic structures.[181,197,198] In one study, shown in **Figure 9**, the specimen (capillary tubes with a thin-slab geometry) thickness was modified by changing the spacer thickness, and the rate of solidification was controlled.[181] Samples of succinonitrile (SCN)–(d)-camphor (DC) eutectic were sealed in 5 mm wide glass sample holders ranging in thickness from 15 to 350 μm. The samples were directionally solidified at a range of velocities and the cross-section perpendicular to the solidification direction was imaged using an optical microscope. The eutectic formed a rod structure independent of the specimen thickness, when high growth velocities were used. This showed that the rod

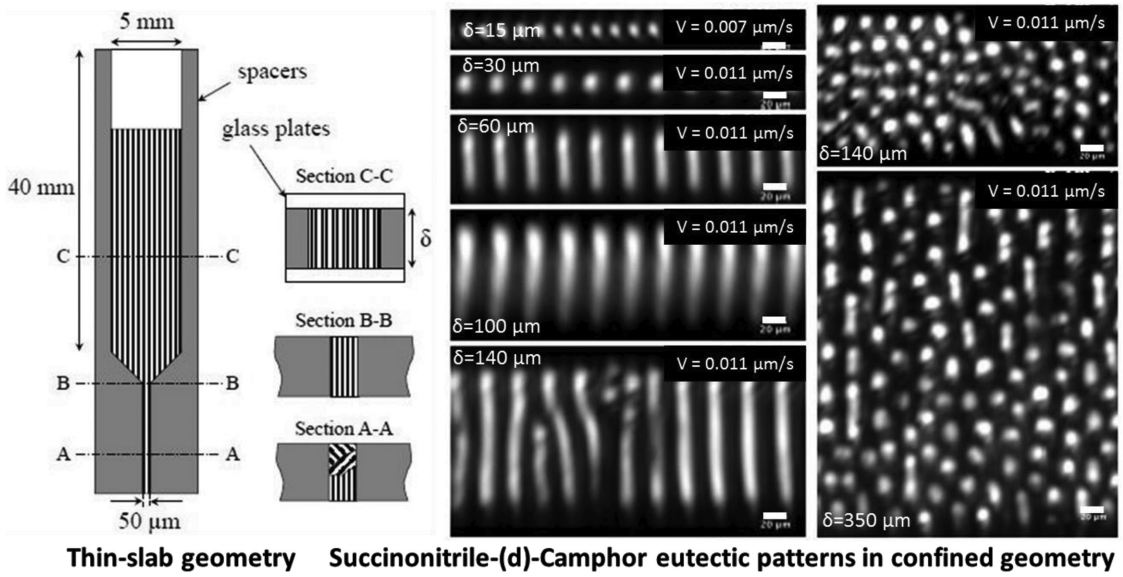

Figure 9. Confinement of eutectics during solidification within a thin slab geometry: Succinonitrile–(d)-camphor eutectic confined in a thin slab geometry with finite thickness (δ). As the thickness varies, the microstructure changes from lamellar to rod morphology. Scale bars 20 μm. Reproduced under the terms of the CC-BY-NC-SA 3.0 license.[181]

morphology was favorable when the characteristic spacing was small. However, at slow growth velocities, the characteristic spacing of the eutectic structure was larger and on the order of the specimen thickness; thus under these conditions, the system can be considered to be "confined." For specimen (confining-geometry) thicknesses between 30 and 140 μm, lamellar patterns of DC and SCN phases are observed. While the volume fraction of SCN–DC would usually result in a rod structure, the ordinarily unfavorable lamellar microstructure formed within a confinement since the lamellar instability modes were blocked as the specimen thickness was smaller than the critical wavelengths of the morphological instability threshold.[177,178] For specimen thicknesses above 140 μm, the bulk microstructure of DC rods in SCN matrix was observed for the same slow growth velocities. These steady-state morphologies that formed at different velocities with the confinement effects of the solidification template showed a bistability in the eutectic pattern. Phase-field modeling was used to confirm these transitions.[177,180,197] Rod-to-lamellar transitions resulting from confinement effects of the template could prove useful in designing specific periodic microstructures in the solidifying eutectic material.

The effect of confinement on the solidification of eutectics has also been studied using microporous AAO as a template. Single-crystal nanowires of Bi–Sn solder eutectic alloy were synthesized by confining its solidification within this porous structure.[199] The AAO templates were infiltrated by the metal eutectics using a setup that enabled evacuating the air from the pores, followed by hydraulic pressure injection of the melt into the pores. The confined Bi–Sn eutectic melt phase-separated within these nanosized pores to form an alternating layer structure (**Figure 10**).[199,200] Given the direction of heat flow (from the top of the template to the bottom surface, where heat is extracted) and the expected solidification direction that results, alternating layers of the eutectic would ordinarily be expected to align along the axis of the cylindrical pores. However, the template-directed eutectic exhibited an unexpected orientation of phase-separation of the Bi and Sn phases. Such phase separation could arise due to the confinement effects of the small pores on the eutectic. It can be observed in Figure 10

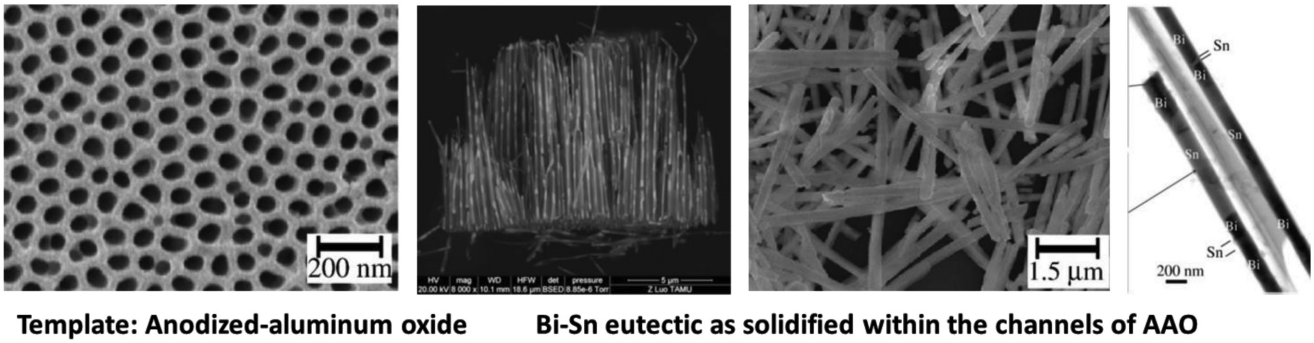

Figure 10. Confinement of eutectic during solidification in AAO template: Bi–Sn eutectic as solidified within the channels of AAO template. This provides a novel approach to synthesize large-area nanowires. Reproduced with permission.[199,200] Copyright 2009, Elsevier.

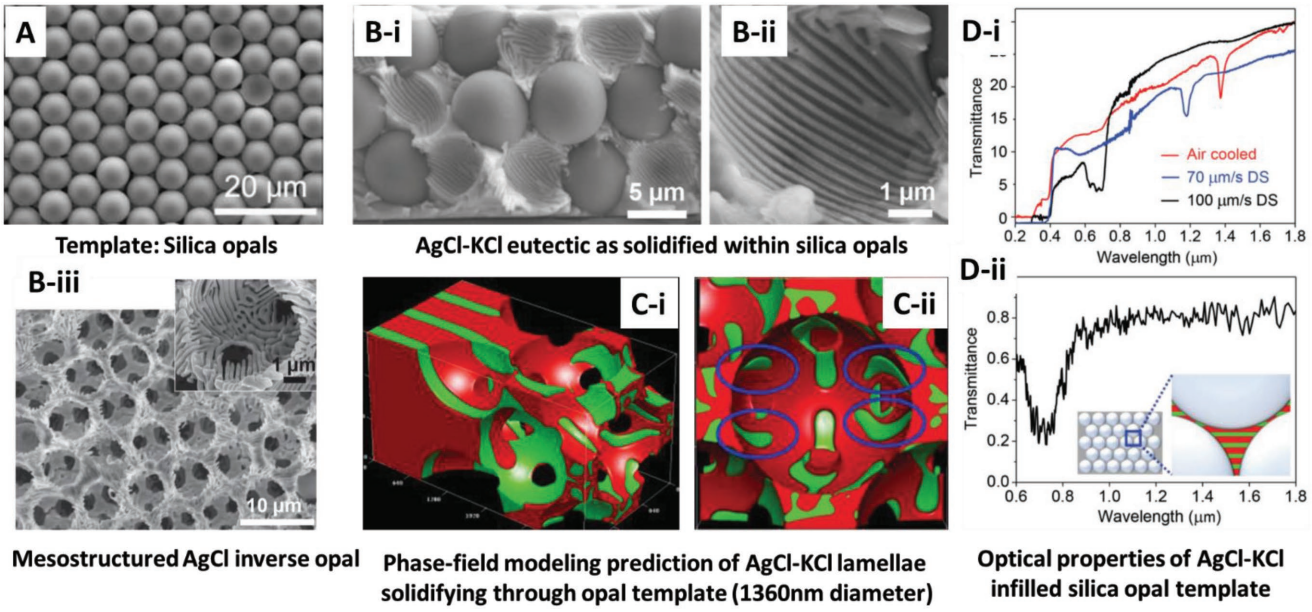

Figure 11. Silica opal template-directed solidification of eutectics: AgCl–KCl eutectic directionally solidified within silica opal template shows a complex morphology of the lamellar eutectic. Reproduced with permission.[93] Copyright 2015, Wiley-VCH.

that there is not a preferred phase that nucleates at the bottom surface of the template; either Bi or Sn can start solidifying at the bottom surface. This leads to a build-up of the atomic species of the other phase, which subsequently solidifies above the first-forming phase. The overall alternating structure does not have a fixed spacing; rather the Bi and Sn layers are of random lengths, suggesting that a stochastic process, such as nucleation, is playing a role. The phase boundary orientation suggests that this phase-separation process is not a traditional directional solidification of a eutectic, where solid-phase separation occurs in a lateral direction, parallel to the solidification front.[14]

The AAO template-directed eutectic solidification presents a novel method to obtain multiphase nanowires of various chemistries, however, lack of control over the thickness of the individual layers could be a concern for optical applications. Future investigations may include eutectic materials of inherent structures such as rods, or spiral, directed by the pores of the AAO template, possibly resulting in helical morphologies.[49]

The confinement of the solidifying eutectic within pores offers a novel method to obtain small feature sizes in the eutectic structure that may not be easy to obtain by simple directional solidification. These pores can also be created via 3D templates, as reported in the case where AgCl–KCl salt eutectic was infiltrated into a silica opal template.[93] The small nanosized gaps between the individual silica colloidal particles gave rise to new morphological features with sizes significantly smaller than that of either the template or the inherent bulk eutectic, as shown in **Figure 11**A,B.[93] The emergence of the 3D mesostructures was mainly determined by the gap size (necks) between the densely packed silica colloidal particles. When the gaps were sufficiently large, the lamellar phase separation was facilitated in such a manner that the eutectic maintained a lamellar structure locally. However, there was no long-range order in the complex morphology of AgCl and KCl lamellae. In the case where this gap size was small, i.e., the colloidal particle diameter was small, a random agglomerate of AgCl and KCl phases was observed with no short- or long-range order.[93]

This 3D mesostructured network of AgCl–KCl eutectic imposed by the template exhibited intriguing optical properties that could be changed by varying the rate of directional solidification. Depending on the lamellar spacing of the mesostructured eutectic, sharp dips in the transmission spectrum were observed around 1.42 μm, 1.18 μm or 690 nm, corresponding to the features in the complex morphology of the template-directed eutectic (Figure 11D).[93] This was confirmed with optical simulations for a simplified structure of alternating dielectric layers (assuming the refractive index of 1.49 and 2.09 for KCl and AgCl, respectively) infiltrated within a matrix of silica spheres. The absence of any optical response from the opal template suggested that the mesostructure retains optical features from the lamellar eutectic, even when infiltrated within a periodic array of silica colloidal particles.[93]

5.3. Challenges and Opportunities of Template-Directed Solidification of Eutectic Materials

There are a large number of material combinations that undergo eutectic solidification.[87,88,91,92,201,202] However, it is challenging to test all of these material chemistries to obtain the desired template-directed eutectic optical materials. Thus, it is critical to select the best material system for a given application and for ease of processing. Processing challenges include limitations of the ambient environment control, undesired chemical reactions, and the thermal and chemical stability of the template materials. The template features should be durable and strong enough to tolerate stresses from volume changes during the melting and solidification of the eutectic materials. In some cases, processes may require rapid heating

or quenching and thus the template materials must be able to survive large thermal gradients.

The ideal template fabrication technique should provide features at the desired length scales. For model studies, lithographic techniques are probably best, given their precision and applicability to a diverse range of geometric designs.[8,203] The ability to incorporate a diverse set of materials is important, as the constituent materials play a major role in controlling heat flow, and therefore the temperature profile imposed on the solidifying eutectic, which often strongly affects the resultant microstructure.[195]

The profile of the solidification front within a template can also be determined by the experimental setup, i.e., the source of heat and the method of heat extraction from the molten eutectic-template composite. The greater the degree of control over heat removal, e.g., cooling rate and direction, the greater the control over the eutectic microstructure. The advancements in the experimental setup (for precise control of the temperature profile) need to be accompanied by the development of in situ characterization techniques as it has now become crucial to observe the kinetics and evolution path of the assembly process.[125,181,198,204]

Another consideration is the compatibility between the template surface and the solidifying eutectic material. Chemical stability and wettability are particularly important for template-directed eutectic solidification. Surface modifications, such as metal or oxide coatings, could provide favorable, stable surface chemistries and allow controlled flow of the liquid eutectic material over the template surface. The template material must also have a melting temperature higher than that of the eutectic temperature to avoid thermal instability or melting of the template. For some applications, it may also be important for the template to be reusable.

For cases when certain materials with desired properties cannot be directly solidified through a template, a template-directed eutectic could itself act as a template for other materials. This can be achieved by selectively etching one of the phases and infiltrating with new materials.[94,205] This replacement technique could be especially advantageous in synthesizing optical metasurfaces and metallodielectric optical metamaterials.

Phase-field simulation of the microstructural evolution in template-directed eutectic solidification can give further insight as both a complement to experiments and as a predictive tool. One benefit realized through simulation is the ability to investigate the isolated effects of each material property or process parameter. For example, one can adjust the eutectic-point phase fraction of a material system in a simulation without changing other parameters ordinarily associated with a material change, such as diffusivity or interfacial energy. This approach allows one to gain understanding of what material properties or process parameters have the largest influence on the resultant microstructure and its ability to facilitate a desired optical response. Simulations also allow the examination of details that are difficult or impossible to observe during experiments, such as the orientation of the solidification front or the specifics of the path of microstructure evolution. Some of these details can be quantified in the simulation, such as the undercooling of the solidification front or the chemical composition distribution in the liquid ahead of the front.

Additionally, simulating the template-directed eutectic solidification can often offer strategies for circumventing challenges that arise in experiments, such as the potential difficulty in controlling the temperature profile of a sample during solidification, issues with eutectic-substrate compatibility, or synthesizing particular template geometry. Overcoming these experimental challenges is sometimes necessary, but using the simulations as a predictive tool to determine promising combinations of template geometries, material properties, and processing parameters narrows the focus of the experimental efforts and thus increases developmental efficiency. In this manner, the cooperation of both experiments and simulations can lead to novel and successful template-directed eutectic optical materials more rapidly than experiments alone.

To this end, we have developed a phase-field model to predict microstructural evolution resulting from the confinement within the template and to investigate template-directed eutectic solidification.[93,166] The approach combines a three-phase eutectic solidification phase-field model with the smoothed boundary method (SBM).[166] The SBM is used to impose no-flux boundary conditions at the diffuse interface of a domain parameter (that indicates the region occupied by the template), capturing the impermeability of the eutectic materials into the template material.

Directional solidification in the simulation is driven by the motion of an imposed linear temperature gradient at a constant speed comparable to the sample pulling velocity in an experiment. More complex temperature profiles can be employed as well, such as those calculated by heat transfer simulations.[94,195] The heat transfer could also be coupled with the eutectic phase-field model directly to track the temperature evolution.

These phase-field simulations can be applied to study the evolution of the microstructure, chemical composition, and undercooling. Perhaps most importantly, the final microstructures formed from directional solidification of a eutectic through a periodic template can be predicted even before an experiment is performed.[93,195] **Figure 12** shows examples of such predicted structures. A 2D simulation predicted a structure formed by

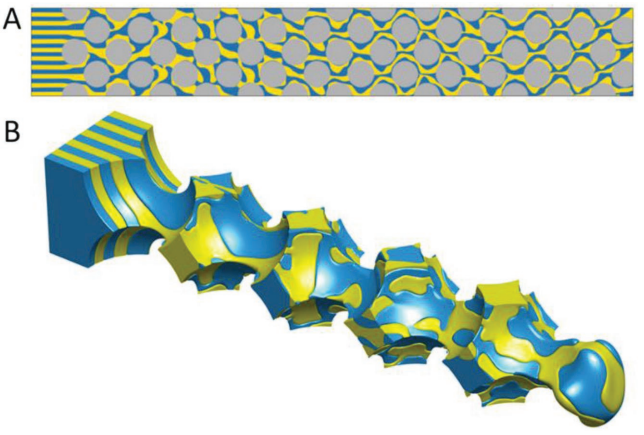

Figure 12. Phase-field simulations of template-directed eutectic solidification: Example microstructures of a 50/50 volume fraction eutectic material solidified through templates. A) 2D simulation with a hexagonally arranged pillar template. B) 3D simulation with a template consisting of spheres arranged in a simple-cubic configuration.

solidifying a 50/50 volume fraction eutectic through a hexagonally arranged lattice of pillars (Figure 12A). The template has a clear effect on the morphology of the eutectic material, as it departs significantly from its inherent lamellar structure. A 3D simulation predicted the structure of the same 50/50 volume fraction eutectic, directionally solidified through the pores of a template consisting of spheres arranged in a simple-cubic lattice (Figure 12B). This simulation once again demonstrates that the resultant microstructure has complexity not present in the intrinsic lamellar structure or the template.[93,195] Furthermore, these structures inherit long-range periodicity that is not present in traditional directionally solidified eutectic materials, providing a path to enabling the desired optical response of these materials.

There are great opportunities in the design space for the template-directed solidification of eutectics to tailor the light–matter interactions for optical metamaterial applications. However, such applications require a high level control over the eutectic morphologies and their degree of order, both at short and long ranges. Along with appropriate template design, this will require precise control over the rate and direction of heat flow in the experimental design, allowing steady-state solidification conditions suitable to produce a high degree of order. If this is realized, the potential list of applications will include optical, electronic, magnetic, thermal, photovoltaic, and mechanical functionalities. To date, reports on template-directed organization of eutectics have been predominantly limited to lamellar eutectic systems. By utilizing other eutectic structures with rod, irregular, or complex motifs, new classes of template-directed eutectic organization can be explored.

6. Conclusions and Outlook

To create new photonic crystals and optical metamaterials with unusual optical properties, novel structures and concepts of fabrication methodologies are required. One way of achieving this is by fabricating metallodielectric nanostructures that could have negative index of refraction and act as left-handed materials in the visible and near-IR spectral ranges.[8,206] Target properties of such nanostructured metamaterials could include invisibility cloaking, optical magnetism, improved imaging (by superlensing or supercollimation), and enhanced light emission and detection.[9] These properties may possibly be realized through the ability of template-directed eutectic solidification to form subwavelength-scale complex microstructures in matter.[4]

Critical to photonic crystals and metamaterials is precise control of microstructure and the materials making up that microstructure. Eutectic systems may be useful in forming some high-symmetry structures, like diamond structures,[207] holey fibers,[208] gyroids,[209] and supercell structures,[210] that have been predicted to act as powerful photonic crystals. Examples of important metamaterial structures include: highly ordered split-ring resonators, helical structures, and fishnets;[4,8,9,40,211] geometries yet to be fabricated and measured for eutectic systems. Realization of templates that provide such structures starting with a eutectic material would be ground breaking in optical material synthesis. The template itself can be used as a primitive photonic crystal, and the solidifying-eutectic structure could be a supercell structure defined by the template.[210,212,213] Top-down fabrication techniques of photolithography, electron-beam lithography, interference lithography, and direct laser-writing have been used to fabricate patterns out of silicon, titania, glass, or polymers, which can also be inverted into metallic templates.[203,214–219] Thus, templates can be fabricated with metals or dielectric materials, and the final template-directed eutectic pattern could possibly be either a metallodielectric or an all-dielectric structure.

Further studies are required to master the art of obtaining large-area morphologies for functional applications. Apart from 2D patterned surface templates,[203] many 3D scaffolds like metal foams, inverse opals, holey fibers, gyroids, helices, and nanowires could possibly be used as templates to fabricate intricate shapes of eutectic materials.[4,9,195,196] Additionally, the concepts from the field of directed assembly of block copolymers could be explored, in which balancing the thermodynamic and kinetic constraints has proven critical in perfecting their final microstructures for target applications.[61,65,220]

The field of template-directed solidification of eutectics is relatively new, and thus we must undertake fundamental solidification studies. We can make use of nanoporous scaffolds like porous silicon, porous glass, and porous anodic alumina membranes,[49,205,221,222] to study the effects of the characteristic length scale of the template (vs the characteristic spacing of the eutectic) on the microstructural evolution. Perhaps some subwavelength metastable structures that could result may be suitable for optical metamaterials.

Phase-field simulations, coupled with well-established optical simulations,[223] can be critical in predicting the expected structures, and useful for designing templates to achieve microstructures specific to the desired optical applications. The developed phase-field model provides an efficient tool to investigate how a structure is influenced by a wide range of variables, including material properties and processing parameters. The model's ability to predict structures is particularly useful in the design of template geometries in the pursuit of well-ordered periodic eutectic structures. Parametric studies of template geometry variables such as spacing, size, arrangement, and shape can be used to screen for promising structures prior to experiments.

In summary, in this review, we focused on the prior results and future opportunities for template-directed organization of eutectic materials and discussed the challenges that will need to be overcome to obtain powerful photonic crystals and optical metamaterials via this approach. The initial results have been significant in understanding the fundamentals of eutectic confinement by templates and the prerequisites for designing a successful template for a specific microstructure. These results have opened new possibilities in the field of template-directed assembly of materials. As a guide for researchers, we have summarized (**Figure 13**) the crucial parameters outlining the criteria to select appropriate eutectic materials and templates to obtain structures for optical applications. There are a number of criteria for template-directed-solidified eutectic materials, each with a specific objective that must be achieved to produce a functional optical material system. By combining a range of experimental techniques and coupling with simulations, the complex goal of designing large-area optical materials with practical

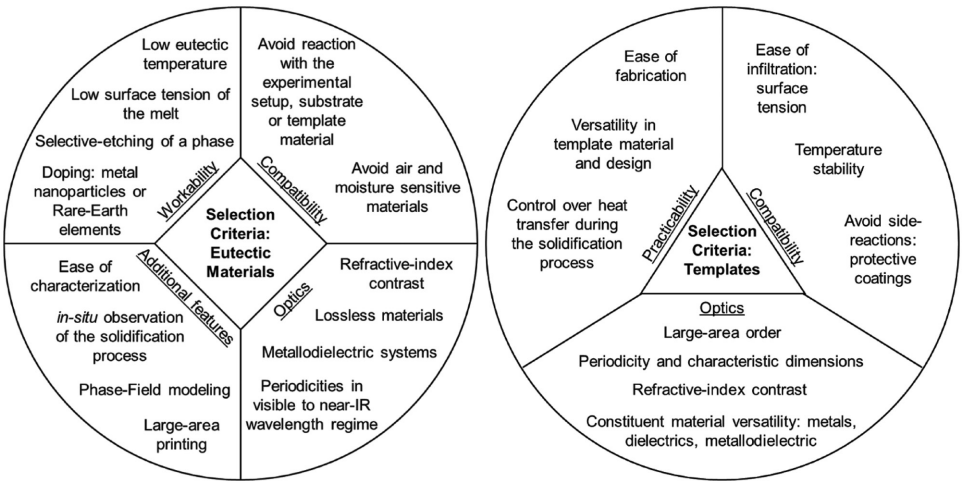

Figure 13. Selection criteria for eutectic materials and templates to obtain structures for optical applications.

performance appears to be within the reach of the research community. Such a multidisciplinary approach will accelerate progress for reaching the ultimate goal of using eutectic solidification to form materials with unprecedented optical properties.

Acknowledgements

The authors acknowledge support through the Air Force Office of Scientific Research (AFOSR) Multidisciplinary University Research Initiative FA9550-12-0471 and helpful discussions with Dr. Ali Sayir (AFOSR). The authors thank the previous group members involved in this research, and the many interactions with Professors Shanhui Fan, Jennifer Lewis, Lane Martin, John Rogers, John Halloran, and Mauricio Terrones and their research groups. This article is part of the *Advanced Optical Materials* Hall of Fame article series, which recognizes the excellent contributions of leading researchers to the field of optical materials science.

Conflict of Interest

The authors declare no conflict of interest.

Keywords

eutectics, metamaterials, organized systems, photonic crystals, template-directed assembly

Received: January 19, 2018
Revised: February 23, 2018
Published online: March 30, 2018

[1] J. D. Joannopoulos, S. G. Johnson, J. N. Winn, R. D. Meade, *Photonic Crystals: Molding the Flow of Light*, Princeton University Press, Princeton, NJ, USA **2011**.
[2] J. D. Joannopoulos, P. R. Villeneuve, S. Fan, *Nature* **1997**, *386*, 143.
[3] M. C. Teich, B. Saleh, *Fundamentals of Photonics*, Vol. *3*, Wiley-Interscience, Canada **1991**.
[4] X. C. Tong, *Functional Metamaterials and Metadevices*, Vol. *262*, Springer, Bolingbrook, IL, USA **2017**.
[5] J. B. Pendry, *Phys. Rev. Lett.* **2000**, *85*, 3966.
[6] Y. Tang, A. E. Cohen, *Phys. Rev. Lett.* **2010**, *104*, 163901.
[7] J. Y. Kim, H. Kim, B. H. Kim, T. Chang, J. Lim, H. M. Jin, J. H. Mun, Y. J. Choi, K. Chung, J. Shin, *Nat. Commun.* **2016**, *7*, 12911.
[8] C. M. Soukoulis, M. Wegener, *Nat. Photonics* **2011**, *5*, 523.
[9] A. M. Urbas, Z. Jacob, L. Dal Negro, N. Engheta, A. Boardman, P. Egan, A. B. Khanikaev, V. Menon, M. Ferrera, N. Kinsey, C. DeVault, J. Kim, V. Shalaev, A. Boltasseva, J. Valentine, C. Pfeiffer, A. Grbic, E. Narimanov, L. Zhu, S. Fan, A. Alu, E. Poutrina, N. M. Litchinitser, M. A. Noginov, K. F. MacDonald, E. Plum, X. Liu, P. F. Nealey, C. R. Kagam, C. B. Murray, D. A. Pawlak, I. I. Smolyaninov, V. N. Smolyaninov, D. Chanda, *J. Optics* **2016**, *18*, 093005.
[10] T. Yatsui, *Nanophotonic Fabrication: Self-Assembly and Deposition Techniques*, Springer Verlag, Berlin **2012**.
[11] B. P. Isaacoff, K. A. Brown, *Nano Lett.* **2017**, *17*, 6508.
[12] J. F. Galisteo-López, M. Ibisate, R. Sapienza, L. S. Froufe-Pérez, Á. Blanco, C. López, *Adv. Mater.* **2011**, *23*, 30.
[13] G. von Freymann, V. Kitaev, B. V. Lotsch, G. A. Ozin, *Chem. Soc. Rev.* **2013**, *42*, 2528.
[14] G. A. Chadwick, *Prog. Mater. Sci.* **1963**, *12*, 99.
[15] A. Noshay, J. E. McGrath, *Block Copolymers: Overview and Critical Survey*, Elsevier Science, Burlington **2013**.
[16] C. De Rosa, C. Park, E. L. Thomas, B. Lotz, *Nature* **2000**, *405*, 433.
[17] R. Elliott, *Int. Met. Rev.* **1977**, *22*, 161.
[18] M. Muthukumar, C. Ober, E. Thomas, *Science* **1997**, *277*, 1225.
[19] H. Zeng, J. Li, J. P. Liu, Z. L. Wang, S. Sun, *Nature* **2002**, *420*, 395.
[20] A. K. Boal, F. Ilhan, J. E. DeRouchey, T. Thurn-Albrecht, T. P. Russell, V. M. Rotello, *Nature* **2000**, *404*, 746.
[21] K.-S. Choi, H. C. Lichtenegger, G. D. Stucky, E. W. McFarland, *J. Am. Chem. Soc.* **2002**, *124*, 12402.
[22] A. Corma, F. Rey, J. Rius, M. J. Sabater, S. Valencia, *Nature* **2004**, *431*, 287.
[23] E. Winfree, F. Liu, L. A. Wenzler, N. C. Seeman, *Nature* **1998**, *394*, 539.
[24] S. M. Douglas, H. Dietz, T. Liedl, B. Högberg, F. Graf, W. M. Shih, *Nature* **2009**, *459*, 414.
[25] B. J. Scott, G. Wirnsberger, G. D. Stucky, *Chem. Mater.* **2001**, *13*, 3140.
[26] W. D. Callister, D. G. Rethwisch, *Materials Science and Engineering*, Vol. *5*, John Wiley & Sons, New York **2011**.
[27] F. Xia, L. Jiang, *Adv. Mater.* **2008**, *20*, 2842.

[28] A. Malshe, K. Rajurkar, A. Samant, H. N. Hansen, S. Bapat, W. Jiang, *CIRP Ann. Manuf. Technol.* **2013**, *62*, 607.
[29] J. Huang, L. Lin, D. Sun, H. Chen, D. Yang, Q. Li, *Chem. Soc. Rev.* **2015**, *44*, 6330.
[30] S. Kim, C. B. Park, *Adv. Funct. Mater.* **2013**, *23*, 10.
[31] P. M. Ajayan, L. S. Schadler, P. V. Braun, *Nanocomposite Science and Technology*, Wiley-VCH, Weinheim, Germany **2003**.
[32] K. Liu, L. Jiang, *Nano Today* **2011**, *6*, 155.
[33] P. V. Braun, P. Wiltzius, *Nature* **1999**, *402*, 603.
[34] J. Kim, H. S. Kim, J. H. Choi, H. Jeon, Y. Yoon, J. Liu, J.-G. Park, P. V. Braun, *Chem. Mater.* **2014**, *26*, 7051.
[35] M. Miyake, M. Suginohara, N. Narahara, T. Hirato, P. V. Braun, *Chem. Mater.* **2017**, *29*, 9734.
[36] J. I. Lee, S. H. Cho, S.-M. Park, J. K. Kim, J. K. Kim, J.-W. Yu, Y. C. Kim, T. P. Russell, *Nano Lett.* **2008**, *8*, 2315.
[37] J. W. Galusha, M. R. Jorgensen, M. H. Bartl, *Adv. Mater.* **2010**, *22*, 107.
[38] W. Zhang, D. Zhang, T. Fan, J. Ding, Q. Guo, H. Ogawa, *Nanotechnology* **2006**, *17*, 840.
[39] D. Kurdyukov, N. F. Kartenko, V. Golubev, *J. Alloys Compd.* **2010**, *492*, 611.
[40] K. A. Arpin, A. Mihi, H. T. Johnson, A. J. Baca, J. A. Rogers, J. A. Lewis, P. V. Braun, *Adv. Mater.* **2010**, *22*, 1084.
[41] S. G. Romanov, C. M. Sotomayor Torres, in *Handbook of Nanostructured Materials and Nanotechnology* (Ed: H. S. Nalwa), Academic Press, Burlington **2000**, p. xxi.
[42] E. Armstrong, C. O'Dwyer, *J. Mater. Chem. C* **2015**, *3*, 6109.
[43] H. Zhang, T. Shi, D. J. Wetzel, R. G. Nuzzo, P. V. Braun, *Adv. Mater.* **2016**, *28*, 742.
[44] J. Liu, Q. Zheng, M. D. Goodman, H. Zhu, J. Kim, N. A. Krueger, H. Ning, X. Huang, J. Liu, M. Terrones, P. V. Braun, *Adv. Mater.* **2016**, *28*, 7696.
[45] S. Kim, J. Liu, K. Sun, J. Wang, S. J. Dillon, P. V. Braun, *Adv. Funct. Mater.* **2017**, *27*, 1702783.
[46] R. Zhang, J. Cohen, S. Fan, P. V. Braun, *Nanoscale* **2017**, *9*, 11187.
[47] D. Wang, V. Salgueirino-Maceira, L. M. Liz-Marzan, F. Caruso, *Adv. Mater.* **2002**, *14*, 908.
[48] H. Masuda, M. Satoh, *Jpn. J. Appl. Phys.* **1996**, *35*, L126.
[49] Y. Wu, G. Cheng, K. Katsov, S. W. Sides, J. Wang, J. Tang, G. H. Fredrickson, M. Moskovits, G. D. Stucky, *Nat. Mater.* **2004**, *3*, 816.
[50] D. Yang, J. Carpena-Nunez, L. F. Fonseca, A. Biaggi-Labiosa, G. W. Hunter, *Sci. Rep.* **2014**, *4*, 3773.
[51] P. Vukusic, J. R. Sambles, *Nature* **2003**, *424*, 852.
[52] A. Blanco, E. Chomski, S. Grabtchak, M. Ibisate, S. John, S. W. Leonard, C. Lopez, F. Meseguer, H. Miguez, J. P. Mondia, G. A. Ozin, O. Toader, H. M. van Driel, *Nature* **2000**, *405*, 437.
[53] Y. A. Vlasov, X.-Z. Bo, J. C. Sturm, D. J. Norris, *Nature* **2001**, *414*, 289.
[54] B. A. Parviz, D. Ryan, G. M. Whitesides, *IEEE Trans. Adv. Packag.* **2003**, *26*, 233.
[55] G. M. Gratson, F. García-Santamaría, V. Lousse, M. Xu, S. Fan, J. A. Lewis, P. V. Braun, *Adv. Mater.* **2006**, *18*, 461.
[56] W. Lee, A. Chan, M. A. Bevan, J. A. Lewis, P. V. Braun, *Langmuir* **2004**, *20*, 5262.
[57] P. Chen, Z. Luo, S. Guven, S. Tasoglu, A. V. Ganesan, A. Weng, U. Demirci, *Adv. Mater.* **2014**, *26*, 5936.
[58] N. V. Dziomkina, G. J. Vancso, *Soft Matter* **2005**, *1*, 265.
[59] A. M. Hung, C. M. Micheel, L. D. Bozano, L. W. Osterbur, G. M. Wallraff, J. N. Cha, *Nat. Nanotechnol.* **2010**, *5*, 121.
[60] D. Wang, H. Möhwald, *J. Mater. Chem.* **2004**, *14*, 459.
[61] J. Y. Cheng, A. M. Mayes, C. A. Ross, *Nat. Mater.* **2004**, *3*, 823.
[62] M. Ramanathan, S Michael Kilbey II, Q. Ji, J. P. Hill, K. Ariga, *J. Mater. Chem.* **2012**, *22*, 10389.
[63] S. O. Kim, H. H. Solak, M. P. Stoykovich, N. J. Ferrier, J. J. de Pablo, P. F. Nealey, *Nature* **2003**, *424*, 411.
[64] C. Park, J. Y. Cheng, M. J. Fasolka, A. M. Mayes, C. A. Ross, E. L. Thomas, C. De Rosa, *Appl. Phys. Lett.* **2001**, *79*, 848.
[65] M. S. Onses, C. Song, L. Williamson, E. Sutanto, P. M. Ferreira, A. G. Alleyne, P. F. Nealey, H. Ahn, J. A. Rogers, *Nat. Nanotechnol.* **2013**, *8*, 667.
[66] H. Yi, X. Y. Bao, R. Tiberio, H. S. P. Wong, *Nano Lett.* **2015**, *15*, 805.
[67] J. Y. Cheng, C. A. Ross, E. L. Thomas, H. I. Smith, G. J. Vancso, *Adv. Mater.* **2003**, *15*, 1599.
[68] J. Fan, S. W. Boettcher, C.-K. Tsung, Q. Shi, M. Schierhorn, G. D. Stucky, *Chem. Mater.* **2007**, *20*, 909.
[69] P. V. Braun, P. Osenar, S. I. Stupp, *Nature* **1996**, *380*, 325.
[70] S. J. Tan, M. J. Campolongo, D. Luo, W. Cheng, *Nat. Nanotechnol.* **2011**, *6*, 268.
[71] Q. Y. Lin, Z. Li, K. A. Brown, M. N. O'Brien, M. B. Ross, Y. Zhou, S. Butun, P. C. Chen, G. C. Schatz, V. P. Dravid, K. Aydin, C. A. Mirkin, *Nano Lett.* **2015**, *15*, 4699.
[72] T. Tigges, T. Heuser, R. Tiwari, A. Walther, *Nano Lett.* **2016**, *16*, 7870.
[73] E. M. Roller, L. K. Khorashad, M. Fedoruk, R. Schreiber, A. O. Govorov, T. Liedl, *Nano Lett.* **2015**, *15*, 1368.
[74] X. Li, J. C. Armas-Pérez, J. P. Hernández-Ortiz, C. G. Arges, X. Liu, J. A. Martínez-González, L. E. Ocola, C. Bishop, H. Xie, J. J. de Pablo, P. F. Nealey, *ACS Nano* **2017**, *11*, 6492.
[75] J. W. Cahn, *Acta Metall.* **1961**, *9*, 795.
[76] J. S. Langer, *Ann. Phys. (N.Y.)* **1971**, *65*, 53.
[77] K. Grönhagen, J. Ågren, M. Odén, *Scr. Mater.* **2015**, *95*, 42.
[78] R. A. L. Jones, L. J. Norton, E. J. Kramer, F. S. Bates, P. Wiltzius, *Phys. Rev. Lett.* **1991**, *66*, 1326.
[79] K. Binder, P. Fratzl, in *Phase Transformations in Materials*, Wiley-VCH, Weinheim, Germany **2001**, p. 409.
[80] V. M. Lopez-Hirata, E. O. Avila-Davila, M.-L. Saucedo-Muñoz, J. D. Villegas-Cardenas, O. Soriano-Vargas, *Mater. Res.* **2017**, *20*, 639.
[81] S. P. Singhal, H. Herman, G. Kostorz, *J. Appl. Crystallogr.* **1978**, *11*, 572.
[82] D. E. Laughlin, J. W. Cahn, *Acta Metall.* **1975**, *23*, 329.
[83] E. Levin, H. McMurdie, F. Hall, *Phase Diagrams for Ceramists*, The American Ceramic Society, Columbus, Ohio **1956**.
[84] Z. Chen, X. Wang, Y. Qi, S. Yang, J. A. N. T. Soares, B. A. Apgar, R. Gao, R. Xu, Y. Lee, X. Zhang, J. Yao, L. W. Martin, *ACS Nano* **2016**, *10*, 10237.
[85] D. A. Pawlak, K. Kolodziejak, S. Turczynski, J. Kisielewski, K. Rożniatowski, R. Diduszko, M. Kaczkan, M. Malinowski, *Chem. Mater.* **2006**, *18*, 2450.
[86] D. A. Pawlak, S. Turczynski, M. Gajc, K. Kolodziejak, R. Diduszko, K. Rozniatowski, J. Smalc, I. Vendik, *Adv. Funct. Mater.* **2010**, *20*, 1116.
[87] J. Hunt, K. Jackson, *Trans. Metall. Soc. AIME* **1966**, *236*, 843.
[88] K. Jackson, J. Hunt, *Trans. Metall. Soc. AIME* **1966**, *236*, 1129.
[89] E. Scheil, *Z. Metallkunde* **1946**, *37*, 123.
[90] E. Scheil, *Z. Metallkunde* **1954**, *45*, 298.
[91] J. Llorca, V. Orera, *Prog. Mater. Sci.* **2006**, *51*, 711.
[92] A. Sayir, in *Computer-Aided Design of High-Temperature Materials* (Eds: A. Pechenik, R. K. Kalia, P. Vashishta), Oxford University Press, Oxford, UK **1999**, p. 197.
[93] J. Kim, L. K. Aagesen, J. H. Choi, J. Choi, H. S. Kim, J. Liu, C. R. Cho, J. G. Kang, A. Ramazani, K. Thornton, P. V. Braun, *Adv. Mater.* **2015**, *27*, 4551.
[94] J. W. Boley, K. Chaudhary, T. J. Ober, M. Khorasaninejad, W. T. Chen, E. Hanson, A. Kulkarni, J. Oh, J. Kim, L. K. Aagesen, A. Y. Zhu, F. Capasso, K. Thornton, P. V. Braun, J. A. Lewis, *Adv. Mater.* **2017**, *29*, 1604778.
[95] J. Pena, R. Merino, N. Harlan, A. Larrea, G. De La Fuente, V. Orera, *J. Eur. Ceram. Soc.* **2002**, *22*, 2595.
[96] J. Lee, A. Yoshikawa, H. Kaiden, K. Lebbou, T. Fukuda, D. Yoon, Y. Waku, *J. Cryst. Growth* **2001**, *231*, 179.

[97] N. Yasui, T. Kobayashi, Y. Ohashi, T. Den, *J. Cryst. Growth* **2014**, *399*, 7.
[98] A. Larrea, L. Contreras, R. I. Merino, J. Llorca, V. M. Orera, *J. Mater. Res.* **2011**, *15*, 1314.
[99] P. B. Oliete, J. I. Peña, A. Larrea, V. M. Orera, J. LLorca, J. Y. Pastor, A. Martín, J. Segurado, *Adv. Mater.* **2007**, *19*, 2313.
[100] H. Okamoto, *Phase Diagrams for Binary Alloys*, Vol. *314*, ASM International, Materials Park, Ohio **2000**.
[101] P. Villars, A. Prince, H. Okamoto, *Handbook of Ternary Alloy Phase Diagrams*, ASM International, Materials Park, Ohio **1995**.
[102] U. R. Kattner, T. B. Massalski, *Binary Alloy Phase Diagrams*, Vol. *147*, ASM International, Materials Park, Ohio **1990**.
[103] F. S. Galasso, *JOM* **1967**, *19*, 17.
[104] F. S. Galasso, F. C. Douglas, J. A. Batt, *JOM* **1970**, *22*, 40.
[105] J. J. Favier, J. P. Morlevat, J. Duvernoy, *Metall. Trans. B* **1983**, *14B*, 105.
[106] N. M. Davis, A. R. Clawson, H. H. Wieder, *Appl. Phys. Lett.* **1969**, *15*, 213.
[107] M. P. M. Colleoni, B. Vidal, *IEEE Trans. Terahertz Sci. Technol.* **2016**, *6*, 757.
[108] J. Choi, A. A. Kulkarni, E. Hanson, D. Bacon-Brown, K. Thornton, P. V. Braun, *Adv. Opt. Mater.* **2018**, https://doi.org/10.1002/adom.201701316 (in press).
[109] V. M. Orera, J. I. Peña, R. I. Merino, J. A. Lázaro, J. A. Vallés, M. A. Rebolledo, *Appl. Phys. Lett.* **1997**, *71*, 2746.
[110] V. M. Orera, Á. Larrea, *Opt. Mater.* **2005**, *27*, 1726.
[111] J. D. Parsons, A. S. Yue, *J. Cryst. Growth* **1981**, *55*, 470.
[112] N. Yasui, Y. Ohashi, T. Kobayashi, T. Den, *Adv. Mater.* **2012**, *24*, 5464.
[113] M. F. Acosta, S. G. Rodrigo, L. Martín-Moreno, C. Pecharromán, R. I. Merino, *Adv. Opt. Mater.* **2017**, *5*, 1600670.
[114] M. Massaouti, A. Basharin, M. Kafesaki, M. Acosta, R. Merino, V. Orera, E. Economou, C. Soukoulis, S. Tzortzakis, *Opt. Lett.* **2013**, *38*, 1140.
[115] J. A. Pardo, J. I. Pena, R. I. Merino, R. Cases, Á. Larrea, V. M. Orera, *J. Non-Cryst. Solids* **2002**, *298*, 23.
[116] C. Müller, T. A. M. Ferenczi, M. Campoy-Quiles, J. M. Frost, D. D. C. Bradley, P. Smith, N. Stingelin-Stutzmann, J. Nelson, *Adv. Mater.* **2008**, *20*, 3510.
[117] F. Simon, S. Clevers, G. Gbabode, N. Couvrat, V. Agasse-Peulon, M. Sanselme, V. Dupray, G. Coquerel, *Cryst. Growth Des.* **2015**, *15*, 946.
[118] K. Sadecka, M. Gajc, K. Orlinski, H. B. Surma, A. Klos, I. Jozwik-Biala, K. Sobczak, P. Dluzewski, J. Toudert, D. A. Pawlak, *Adv. Opt. Mater.* **2015**, *3*, 381.
[119] S. Akamatsu, S. Bottin-Rousseau, M. Şerefoğlu, G. Faivre, *Acta Mater.* **2012**, *60*, 3206.
[120] P. Villars, H. Okamoto, K. Cenzual, *ASM Alloy Phase Diagrams Database*, ASM International, Materials Park, Ohio **2016**.
[121] E. Cubukcu, K. Aydin, E. Ozbay, S. Foteinopoulou, C. M. Soukoulis, *Nature* **2003**, *423*, 604.
[122] I. Yamada, K. Takano, M. Hangyo, M. Saito, W. Watanabe, *Opt. Lett.* **2009**, *34*, 274.
[123] M. G. Day, A. Hellawell, *Proc. R. Soc. London, Ser. A* **1968**, *305*, 473.
[124] A. Hellawell, *Trans. Metall. Soc. AIME* **1967**, *239*, 1049.
[125] A. J. Shahani, X. Xiao, P. W. Voorhees, *Nat. Commun.* **2016**, *7*, 12953.
[126] Z. Ebrahimi, *Arch. Metall. Mater.* **2017**, *62*, 1969.
[127] A. Cerjan, S. Fan, *New J. Phys.* **2016**, *18*, 125007.
[128] A. Cerjan, S. Fan, *Phys. Rev. Lett.* **2017**, *118*, 253902.
[129] A. Cerjan, S. Fan, *Phys. Rev. A* **2016**, *94*, 033857.
[130] A. Cerjan, A. Raman, S. Fan, *Phys. Rev. Lett.* **2016**, *116*, 203902.
[131] C. D. Adams, D. J. Srolovitz, M. Atzmon, *J. Appl. Phys.* **1993**, *74*, 1707.
[132] I. Petrov, P. B. Barna, L. Hultman, J. E. Greene, *J. Vac. Sci. Technol. A* **2003**, *21*, S117.
[133] K. Fukutani, K. Tanji, T. Saito, T. Den, *J. Appl. Phys.* **2005**, *98*, 033507.
[134] W. Lu, D. Kim, *Acta Mater.* **2005**, *53*, 3689.
[135] H.-C. Yu, W. Lu, *Acta Mater.* **2005**, *53*, 1799.
[136] T. Takaki, T. Hasebe, Y. Tomita, *J. Cryst. Growth* **2006**, *287*, 495.
[137] L. Tan, N. Zabaras, *J. Comput. Phys.* **2007**, *221*, 9.
[138] X.-F. Wu, Y. A. Dzenis, *Phys. Rev. E* **2008**, *77*, 031807.
[139] L. Gránásy, G. Tegze, G. I. Tóth, T. Pusztai, *Philos. Mag.* **2011**, *91*, 123.
[140] B. Sadtler, S. P. Burgos, N. A. Batara, J. A. Beardslee, H. A. Atwater, N. S. Lewis, *Proc. Natl. Acad. Sci. USA* **2013**, *110*, 19707.
[141] A. Bhattacharya, A. Kiran, S. Karagadde, P. Dutta, *J. Comput. Phys.* **2014**, *262*, 217.
[142] A. Fang, K. H. Anna, A. Grosskopf, J. E. Anthony, Y.-L. Loo, M. Haataja, *APL Mater.* **2015**, *3*, 036107.
[143] N. G. Almarza, J. Pekalski, A. Ciach, *Soft Matter* **2016**, *12*, 7551.
[144] L.-X. Lu, Y.-M. Wang, B. M. Srinivasan, M. Asbahi, J. K. W. Yang, Y.-W. Zhang, *Sci. Rep.* **2016**, *6*, 32398.
[145] A. Fang, M. Haataja, *J. Electrochem. Soc.* **2017**, *164*, D875.
[146] J. D. Hill, P. C. Millett, *Sci. Rep.* **2017**, *7*, 5250.
[147] H.-Y. Hsu, B.-T. Lin, Y.-R. Hsu, *Adv. Mech. Eng.* **2017**, *9*, https://doi.org/10.1177/1687814016683357.
[148] R. Kurita, *Sci. Rep.* **2017**, *7*, 6912.
[149] K. Thornton, J. Ågren, P. W. Voorhees, *Acta Mater.* **2003**, *51*, 5675.
[150] G. Boussinot, C. Hüter, E. A. Brener, *Phys. Rev. E* **2011**, *83*, 020601.
[151] J. D. van der Waals, *J. Stat. Phys.* **1979**, *20*, 200.
[152] S. G. Kim, W. T. Kim, T. Suzuki, *Phys. Rev. E* **1999**, *60*, 7186.
[153] A. Karma, W. J. Rappel, *Phys. Rev. E* **1996**, *53*, R3017.
[154] J. W. Cahn, J. E. Hilliard, *J. Chem. Phys.* **1959**, *31*, 688.
[155] N. Provatas, K. Elder, in *Phase-Field Methods in Materials Science and Engineering*, Wiley-VCH, Weinheim, Germany **2010**, p. 33.
[156] S. M. Allen, J. W. Cahn, *Acta Metall.* **1979**, *27*, 1085.
[157] R. Kobayashi, *Physica D* **1993**, *63*, 410.
[158] G. Caginalp, *Arch. Ration. Mech. Anal.* **1986**, *92*, 205.
[159] A. A. Wheeler, W. J. Boettinger, G. B. McFadden, *Phys. Rev. A* **1992**, *45*, 7424.
[160] J. E. Guyer, W. J. Boettinger, J. A. Warren, G. B. McFadden, *Phys. Rev. E* **2004**, *69*, 021603.
[161] J. E. Guyer, W. J. Boettinger, J. A. Warren, G. B. McFadden, *Phys. Rev. E* **2004**, *69*, 021604.
[162] B. Nestler, A. A. Wheeler, *Physica D* **2000**, *138*, 114.
[163] M. Apel, B. Boettger, H. J. Diepers, I. Steinbach, *J. Cryst. Growth* **2002**, *237*, 154.
[164] R. Folch, M. Plapp, *Phys. Rev. E* **2003**, *68*, 010602.
[165] S. G. Kim, W. T. Kim, T. Suzuki, M. Ode, *J. Cryst. Growth* **2004**, *261*, 135.
[166] R. Folch, M. Plapp, *Phys. Rev. E* **2005**, *72*, 011602.
[167] A. Karma, *Phys. Rev. Lett.* **2001**, *87*, 115701.
[168] G. Boussinot, E. A. Brener, *Phys. Rev. E* **2014**, *89*, 060402.
[169] M. Ohno, T. Takaki, Y. Shibuta, *Phys. Rev. E* **2017**, *96*, 033311.
[170] A. Karma, *Phys. Rev. E* **1994**, *49*, 2245.
[171] K. R. Elder, F. Drolet, J. M. Kosterlitz, M. Grant, *Phys. Rev. Lett.* **1994**, *72*, 677.
[172] K. R. Elder, J. D. Gunton, M. Grant, *Phys. Rev. E* **1996**, *54*, 6476.
[173] A. A. Wheeler, G. B. McFadden, W. J. Boettinger, *Proc. R. Soc. London, Ser. A* **1996**, *452*, 495.
[174] M. Plapp, A. Karma, *Phys. Rev. E* **2002**, *66*, 061608.
[175] S. Akamatsu, G. Faivre, M. Plapp, A. Karma, *Metall. Mater. Trans. A* **2004**, *35*, 1815.
[176] J. R. Green, P. K. Jimack, A. M. Mullis, *Metall. Mater. Trans. A* **2007**, *38*, 1426.
[177] A. Parisi, M. Plapp, *Acta Mater.* **2008**, *56*, 1348.
[178] A. Parisi, M. Plapp, *Europhys. Lett.* **2010**, *90*, 26010.
[179] M. Plapp, A. Karma, *Phys. Rev. E* **1999**, *60*, 6865.
[180] M. Şerefoğlu, R. E. Napolitano, M. Plapp, *Phys. Rev. E* **2011**, *84*, 011614.

[181] M. Şerefoğlu, S. Bottin-Rousseau, S. Akamatsu, G. Faivre, *IOP Conf. Ser.: Mater. Sci. Eng.* **2012**, *27*, 012030.
[182] S. Ghosh, M. Plapp, *Acta Mater.* **2017**, *140*, 140.
[183] A. Lahiri, C. Tiwary, K. Chattopadhyay, A. Choudhury, *Comput. Mater. Sci.* **2017**, *130*, 109.
[184] A. Zhang, Z. Guo, S. M. Xiong, *J. Appl. Phys.* **2017**, *121*, 125101.
[185] O. Kazemi, G. Hasemann, M. Krüger, T. Halle, *IOP Conf. Ser.: Mater. Sci. Eng.* **2016**, *118*, 012028.
[186] A. Choudhury, M. Plapp, B. Nestler, *Phys. Rev. E* **2011**, *83*, 051608.
[187] J. Hötzer, M. Jainta, P. Steinmetz, B. Nestler, A. Dennstedt, A. Genau, M. Bauer, H. Köstler, U. Rüde, *Acta Mater.* **2015**, *93*, 194.
[188] J. Hötzer, P. Steinmetz, M. Jainta, S. Schulz, M. Kellner, B. Nestler, A. Genau, A. Dennstedt, M. Bauer, H. Köstler, U. Rüde, *Acta Mater.* **2016**, *106*, 249.
[189] H.-S. Lee, Y.-S. Lee, J.-Y. Suh, M. Kim, J.-S. Yu, Y. W. Cho, *J. Phys. Chem. C* **2011**, *115*, 20027.
[190] X. Liu, D. Peaslee, T. P. Sheehan, E. H. Majzoub, *J. Phys. Chem. C* **2014**, *118*, 27265.
[191] E. Roedern, B. R. S. Hansen, M. B. Ley, T. R. Jensen, *J. Phys. Chem. C* **2015**, *119*, 25818.
[192] K. C. Hugo, *J. Phys.: Condens. Matter* **2001**, *13*, R95.
[193] M. Sliwinska-Bartkowiak, M. Jazdzewska, M. Trafas, M. Kaczmarek-Klinowska, K. E. Gubbins, *J. Chem. Eng. Data* **2015**, *60*, 3093.
[194] J. Hunt, J. Chilton, *J. Inst. Met.* **1963**, *91*, 338.
[195] Z. Yan, M. Han, Y. Shi, A. Badea, Y. Yang, A. Kulkarni, E. Hanson, M. E. Kandel, X. Wen, F. Zhang, Y. Luo, Q. Lin, H. Zhang, X. Guo, Y. Huang, K. Nan, S. Jia, A. W. Oraham, M. B. Mevis, J. Lim, X. Guo, M. Gao, W. Ryu, J. K. Yu, B. G. Nicolau, A. Petronico, S. S. Rubakhin, J. Lou, P. M. Ajayan, K. Thornton, G. Popescu, D. Fang, J. V. Sweedler, P. V. Braun, H. Zhang, R. G. Nuzzo, Y. Huang, Y. Zhang, J. A. Rogers, *Proc. Natl. Acad. Sci. USA* **2017**, *114*, E9455.
[196] S. Xu, Z. Yan, K.-I. Jang, W. Huang, H. Fu, J. Kim, Z. Wei, M. Flavin, J. McCracken, R. Wang, A. Badea, Y. Liu, D. Xiao, G. Zhou, J. Lee, H. U. Chung, H. Cheng, W. Ren, A. Banks, X. Li, U. Paik, R. G. Nuzzo, Y. Huang, Y. Zhang, J. A. Rogers, *Science* **2015**, *347*, 154.
[197] M. Plapp, S. Bottin-Rousseau, G. Faivre, S. Akamatsu, *C. R. Méc.* **2017**, *345*, 56.
[198] M. Serefoglu, R. E. Napolitano, *Acta Mater.* **2008**, *56*, 3862.
[199] S.-H. Chen, C.-C. Chen, Z. P. Luo, C.-G. Chao, *Mater. Lett.* **2009**, *63*, 1165.
[200] S. H. Chen, C. C. Chen, C. G. Chao, *J. Alloys Compd.* **2009**, *481*, 270.
[201] U. Hecht, L. Gránásy, T. Pusztai, B. Böttger, M. Apel, V. Witusiewicz, L. Ratke, J. De Wilde, L. Froyen, D. Camel, B. Drevet, G. Faivre, S. Fries, B. Legendre, S. Rex, *Mater. Sci. Eng. R* **2004**, *46*, 1.
[202] J. Hunt, K. Jackson, *Trans. Metall. Soc. AIME* **1967**, *239*, 864.
[203] M. Khorasaninejad, F. Capasso, *Science* **2017**, *358*, 1146.
[204] A. S. Powers, H. G. Liao, S. N. Raja, N. D. Bronstein, A. P. Alivisatos, H. Zheng, *Nano Lett.* **2017**, *17*, 15.
[205] M. Steinhart, J. Wendorff, A. Greiner, R. Wehrspohn, K. Nielsch, J. Schilling, J. Choi, U. Gösele, *Science* **2002**, *296*, 1997.
[206] V. M. Shalaev, *Nat. Photonics* **2007**, *1*, 41.
[207] M. Maldovan, E. L. Thomas, *Nat. Mater.* **2004**, *3*, 593.
[208] A. F. Oskooi, J. Joannopoulos, S. G. Johnson, *Opt. Express* **2009**, *17*, 10082.
[209] H. Men, K. Y. Lee, R. M. Freund, J. Peraire, S. G. Johnson, *Opt. Express* **2014**, *22*, 22632.
[210] A. Cerjan, S. Fan, *Phys. Rev. A* **2017**, *96*, 051802.
[211] S. Y. Lin, J. G. Fleming, D. L. Hetherington, B. K. Smith, R. Biswas, K. M. Ho, M. M. Sigalas, W. Zubrzycki, S. R. Kurtz, J. Bur, *Nature* **1998**, *394*, 251.
[212] F. Costa, A. Monorchio, G. Manara, *Appl. Comput. Electromagn. Soc. J.* **2014**, *29*, 960.
[213] A. Fallahi, *D.Sc. Thesis*, Swiss Federal Institute of Technology, Zurich **2010**.
[214] Y. Chen, J. GeddesIII, J. Lee, P. Braun, P. Wiltzius, *Appl. Phys. Lett.* **2007**, *91*, 241103.
[215] S. Peng, R. Zhang, V. H. Chen, E. T. Khabiboulline, P. Braun, H. A. Atwater, *ACS Photonics* **2016**, *3*, 1131.
[216] R. Zhang, H. Ning, N. A. Krueger, D. Bacon-Brown, P. V. Braun, *Adv. Opt. Mater.* **2016**, *4*, 1533.
[217] M. Deubel, G. Von Freymann, M. Wegener, S. Pereira, K. Busch, C. M. Soukoulis, *Nat. Mater.* **2004**, *3*, 444.
[218] S. Kawata, H.-B. Sun, T. Tanaka, K. Takada, *Nature* **2001**, *412*, 697.
[219] M. Khorasaninejad, W. T. Chen, A. Y. Zhu, J. Oh, R. C. Devlin, C. Roques-Carmes, I. Mishra, F. Capasso, *IEEE J. Sel. Top. Quantum Electron.* **2017**, *23*, 1.
[220] G. W. Yang, G. P. Wu, X. Chen, S. Xiong, C. G. Arges, S. Ji, P. F. Nealey, X. B. Lu, D. J. Darensbourg, Z. K. Xu, *Nano Lett.* **2017**, *17*, 1233.
[221] N. A. Krueger, A. L. Holsteen, S.-K. Kang, C. R. Ocier, W. Zhou, G. Mensing, J. A. Rogers, M. L. Brongersma, P. V. Braun, *Nano Lett.* **2016**, *16*, 7402.
[222] Z. Y. Deng, H. Fernandes, J. Ventura, S. Kannan, J. M. Ferreira, *J. Am. Ceram. Soc.* **2007**, *90*, 1265.
[223] B. Gallinet, J. Butet, O. J. F. Martin, *Laser Photonics Rev.* **2015**, *9*, 577.